Discovery of a functionally selective ghrelin receptor ($GHSR_{1a}$) ligand for modulating brain dopamine

J. D. Gross[a], D. W. Kim[b], Y. Zhou[a], D. Jansen[b], L. M. Slosky[a], N. B. Clark[a], C. R. Ray[a], X. Hu[b], N. Southall[b], A. Wang[b], X. Xu[b], E. Barnaeva[b], W. C. Wetsel[c,d], M. Ferrer[b], J. J. Marugan[b,1], M. G. Caron[a,1], L. S. Barak[a,1], and K. Toth[a,2]

[a]Department of Cell Biology, Duke University Medical Center, Durham, NC 27710; [b]National Center for Advancing Translational Sciences, NIH Division of Preclinical Innovation, Rockville, MD 20892; [c]Department of Psychiatry and Behavioral Sciences, Duke University Medical Center, Durham, NC 27710; and [d]Mouse Behavioral and Neuroendocrine Analysis Core Facility, Duke University Medical Center, Durham, NC 27710

Edited by Brian Kobilka, Stanford University School of Medicine, Stanford, CA; received July 6, 2021; accepted January 26, 2022

The growth hormone secretagogue receptor-1a ($GHSR_{1a}$) is the cognate G protein–coupled receptor (GPCR) for the peptide hormone ghrelin. $GHSR_{1a}$ is a promising therapeutic target for a wide range of metabolic, age-related, and central nervous system (CNS)–based conditions. In addition, growing evidence supports that $GHSR_{1a}$ is a modulator of dopamine (DA) homeostasis and is neuroprotective within brain DA circuits. $GHSR_{1a}$ signaling originates from pharmacologically separable G protein– and β-arrestin (βarr)–dependent pathways, and consequently, $GHSR_{1a}$-mediated physiological responses depend upon their distinctive signaling contributions. Thus, when treating disorders of disrupted DA homeostasis, a pharmacological strategy that modulates biased $GHSR_{1a}$ signaling may uncouple desired therapeutic outcomes from unwanted side effects. Here, we report the discovery of a small molecule $GHSR_{1a}$ agonist, N8279 (NCATS-SM8864), functionally selective for G protein signaling. Comprehensive pharmacological characterization reveals that N8279 elicits potent $G\alpha_q$ activity at the apo- and ghrelin-bound $GHSR_{1a}$. Further biochemical analysis and molecular modeling demonstrate that N8279 signaling requires the extracellular domain of $GHSR_{1a}$, especially extracellular loop 2. Collectively, these findings suggest that N8279 possesses an extended binding mode into the extracellular vestibule of the $GHSR_{1a}$ that preferentially favors $G\alpha_q$ signaling over alternative G proteins and βarr2-dependent cellular responses. Critically, N8279 is brain-penetrant in mice, exhibits CNS stability, and attenuates dysfunctional DA-mediated behaviors in both genetic and pharmacological mouse models of hyperdopaminergia. Our findings provide insight into the mechanisms governing GPCR functional selectivity and emphasize how biased ligand drug development can produce novel $GHSR_{1a}$ pharmacotherapeutics to treat pathological disruptions of brain DA homeostasis.

NCATS-SM8864 | functional selectivity | GPCR | ghrelin | dopamine

Ghrelin is a peptide hormone secreted from gastric cells during energy deprivation to mediate food-seeking behavior and restore physiological homeostasis (1, 2). Ghrelin exerts its effects via activation of the growth hormone secretagogue receptor-1a ($GHSR_{1a}$), a G protein–coupled receptor (GPCR) (3). In the brain, the $GHSR_{1a}$ is expressed most highly in agouti-related protein (AgRP)/neuropeptide Y (NPY) neurons of the hypothalamic arcuate nucleus and regulates feeding, energy balance, and metabolism (4). In extrahypothalamic regions, $GHSR_{1a}$ is expressed predominantly in the hippocampus, where it regulates learning and cognition (5), and in dopaminergic midbrain neurons, including the mesolimbic dopamine (DA) neurons of the ventral tegmental area (VTA) and nigrostriatal DA neurons of the substantia nigra pars compacta (SNc) (6, 7). Within DAergic cells, $GHSR_{1a}$ acts as a DA neuromodulator through its effect(s) on neuronal firing rate and DA release probability, biochemical processes that influence locomotion, reward-seeking behavior, and cellular health/neuroprotection (6, 8, 9).

Disruptions to central nervous system (CNS) DA homeostasis can lead to psychiatric, neurological, and neurodegenerative conditions (10). While DA-directed pharmacotherapies (e.g., levodopa, DA receptor agonists/antagonists) may benefit patients initially, these approaches often produce unacceptable side effects when administered chronically (11, 12). These unwanted consequences are due, in part, to the challenges of developing selective DA receptor modulators, as well as the inability of these therapeutic strategies to fully restore DA signaling to healthy, homeostatic levels. Accordingly, endogenous DA neuromodulators, such as the ghrelin-$GHSR_{1a}$ system, may provide a more fine-tuned and safer pharmacological means to normalize the dysfunctional DA signaling underlying brain disorders of mood, cognition, or movement, including addiction, Alzheimer's disease (AD), and/or Parkinson's disease (PD) (13, 14).

In peripheral tissue, $GHSR_{1a}$ is essential for a diverse array of physiological processes, including glucose-insulin homeostasis, gastrointestinal motility, cardiovascular health, inflammation, and tissue growth and repair (15). In contrast, $GHSR_{1a}$ activity in the CNS appears less well-defined and may

Significance

The modulation of growth hormone secretagogue receptor-1a ($GHSR_{1a}$) signaling is a promising strategy for treating brain conditions of metabolism, aging, and addiction. $GHSR_{1a}$ activation results in pleiotropic physiological outcomes through distinct and pharmacologically separable G protein– and β-arrestin (βarr)–dependent signaling pathways. Thus, pathway-selective modulation can enable improved pharmacotherapeutics that can promote therapeutic efficacy while mitigating side effects. Here, we describe the discovery of a brain-penetrant small molecule, N8279 (NCATS-SM8864), that biases $GHSR_{1a}$ conformations toward $G\alpha_q$ activation and reduces aberrant dopaminergic behavior in mice. N8279 represents a promising chemical scaffold to advance the development of better treatments for $GHSR_{1a}$-related brain disorders involving the pathological dysregulation of dopamine.

Author contributions: J.D.G., D.W.K., Y.Z., D.J., W.C.W., M.F., J.J.M., M.G.C., L.S.B., and K.T. designed research; J.D.G., D.W.K., Y.Z., D.J., N.B.C., X.H., A.W., X.X., E.B., and K.T. performed research; D.W.K., D.J., and C.R.R. contributed new reagents/analytic tools; J.D.G., D.W.K., Y.Z., D.J., L.M.S., N.B.C., N.S., W.C.W., M.F., J.J.M., M.G.C., L.S.B., and K.T. analyzed data; and J.D.G., W.C.W., J.J.M., M.G.C., L.S.B., and K.T. wrote the paper.

Competing interest statement: A provisional patent application has been deposited with the USPTO by Duke University. A decision on whether to file a formal application will be decided upon in 2022.

This article is a PNAS Direct Submission.

[1]To whom correspondence may be addressed. Email: maruganj@mail.nih.gov, marc.caron@duke.edu, or lawrence.barak@duke.edu.

[2]Present address: Pharmaceutical Sciences, Campbell University, Buies Creek, NC 27506.

This article contains supporting information online at http://www.pnas.org/lookup/suppl/doi:10.1073/pnas.2112397119/-/DCSupplemental.

Published March 3, 2022.

be species- and disorder-dependent (16, 17). For instance, $GHSR_{1a}$(s) expressed in blood–brain barrier (BBB)–protected regions, including the VTA and SNc, may be poorly accessible to the $GHSR_{1a}$-active form of circulating ghrelin (acyl-ghrelin) and many synthetic $GHSR_{1a}$ agonists when administered peripherally (18). Conversely, the hypothalamus and brainstem are surrounded by fenestrated capillaries that enable circulating acyl-ghrelin to reach $GHSR_{1a}$(s) expressed in these regions (17). Thus, $GHSR_{1a}$-targeted neurotherapeutics for DA-based brain disorders must be 1) BBB penetrant in order to modulate hippocampal, mesolimbic, and/or nigrostriatal $GHSR_{1a}$ functions as well as 2) efficacious and bearing a selective therapeutic profile that minimizes on- and off-target side effects.

$GHSR_{1a}$ signals principally through $G\alpha_{q/11}$, but it is also capable of engaging heterotrimeric G proteins within the $G\alpha_{i/o}$ and $G\alpha_{12/13}$ families (19). In addition, $GHSR_{1a}$ elicits β-arrestin (βarr)–dependent cellular responses in a temporally and spatially distinct manner from G protein–mediated signaling, including $GHSR_{1a}$ desensitization, internalization, endocytic trafficking and recycling, and the activation of kinases and transcription factors (20, 21). Thus, $GHSR_{1a}$-directed cellular responses vary according to the extent by which each pathway is selectively activated (ligand selectivity) and modulated downstream (pathway selectivity) (22–24). Most notably, point mutations to adjacent amino acids of the $GHSR_{1a}$ intracellular loop 2 (ICL2), located near the highly conserved E/DRY motif, induce functionally selective G protein or βarr signaling (20, 21). Thus, it may be possible to pharmacologically stabilize $GHSR_{1a}$ into a conformation that selectively activates signaling through one or more of these pathways.

In this study, we present the synthesis and characterization of a $G\alpha_q$-biased $GHSR_{1a}$ agonist, **N8279** (NCATS-SM8864), that contains a 2-carboxamide-3-benzoyl-4-chromenone backbone. In vitro and in silico analyses reveal that **N8279** is functionally selective at $GHSR_{1a}$, and its activity is mediated, at least in part, by extracellular loop 2 (ECL2) and related determinants in the receptor extracellular domain (ECD). In mice, **N8279** readily penetrates the BBB and reaches pharmacologically active levels in brain for extended, druggable periods of time. In vivo efficacy studies show that **N8279** attenuates hyperlocomotion in DA transporter (DAT) knockout (KO) and cocaine-sensitized C57BL/6J mice—both mouse models of hyperDAergia—but it does not affect novelty-related locomotor activity in inbred C57BL/6J mice under normal physiological conditions. Collectively, our findings support that functional selectivity is a promising strategy when designing $GHSR_{1a}$ treatments that target pathophysiological changes in CNS DA homeostasis.

Results

Discovery of a $GHSR_{1a}$-Selective Small Molecule, N8279, by High-Throughput $GHSR_{1a}$ Screening and Structural Characterization. To discover biased $GHSR_{1a}$ ligands, a cell-based, human $GHSR_{1a}$/βarr1 chemiluminescent assay (DiscoverX, PathHunter) was used to screen ∼47,000 compounds from the Sytravon library and the National Center for Advancing Translational Sciences (NCATS) pharmacological collection (NPC) (*SI Appendix*, Fig. S1*A*). We identified 36 hits (0.09% hit rate) with activities greater than 50% of the activity shown by the full length, human acyl-ghrelin peptide (1–28, amino acids) (*SI Appendix*, Fig. S2). Structure-cluster analysis of the hits revealed six chemical scaffolds from the 36 compounds. The hit compounds were reassessed in secondary assays for $G\alpha_{q/11}$-dependent, intracellular Ca^{2+} mobilization (iCa^{2+}) and $\beta arr2^{GFP}$ (green fluorescent protein) translocation (*SI Appendix*, Table S1). From these experiments, NCGC141956 (**N1956**) (*SI Appendix*, Fig. S1*B* and Table S1) was selected for further characterization based on its submicromolar potency and full efficacy relative to the unbiased, small molecule $GHSR_{1a}$ agonist, L692,585 (L585). A further directed library screen of commercial **N1956** analogs identified NCGC00136164 (**N6164**), which unexpectedly, was determined to be a $G\alpha_{q/11}$-biased $GHSR_{1a}$ agonist relative to βarr2 translocation (*SI Appendix*, Table S1). However, the activity of **N1956** and **N6164** could not be confirmed upon resynthesizing these molecules. A liquid chromatography-mass spectrometer (LC-MS) examination of the dimethyl sulfoxide (DMSO) aliquots used in the screening campaign disclosed impurities within **N1956** and **N6164** solutions, corresponding to oxidated derivatives of the 1-phenyl-chromeno-pyrrole-dione scaffold. Further characterization, investigation using NMR and MS methods (*SI Appendix*, Table S2), and resynthesis of pure oxidated products resulted in the determination of the active molecule, **N8279** (NCATS-SM8864) (Fig. 1*A* and *SI Appendix*, Fig. S1*C*), which contains a 2-carboxamide-3-benzoyl-4-chromenone backbone. In solution, **N8279** equilibrates between open and closed conformers, which in specific solvents and conditions can be observed by ^{1}H NMR (*SI Appendix*, Table S2). The structure of the active, open form of **N8279** was confirmed by single crystal X-ray diffraction (Fig. 1*B* and *SI Appendix*, Table S2).

To determine target selectivity, **N8279** activity was evaluated across "the 320 receptor, human GPCRome" by high-throughput screening with a βarr2 recruitment assay (Tango) (25). Hits were defined as ≥3-fold activation above baseline. **N8279** stimulated ∼6-fold activation at $GHSR_{1a}$ and did not exceed ≥3-fold activation at any other GPCR (Fig. 1*C*). The assay quality can be assessed by plotting duplicate, independent trial averages (derived from four independent wells) for each receptor as a point (X, Y). The corresponding plot of points for an ideal assay would be fit by a regression line with the slope = 1. A plot of the assay points produced a regression line with slope of 0.98 (Fig. 1*D*) and is shown with its accompanying 99% prediction band that contains $GHSR_{1a}$ as the only hit. Next, the relative affinity of **N8279** for the $hGHSR_{1a}^{WT}$ ($GHSR_{1a}$) was determined by radioligand binding with [^{125}I]ghrelin. Initial saturation studies confirmed that [^{125}I]ghrelin bound $GHSR_{1a}$ asymptotically with nanomolar affinity (*SI Appendix*, Fig. S3*A*). Subsequent competition binding using [^{125}I]ghrelin at its ∼K_d demonstrate that both unlabeled ghrelin and **N8279** displace [^{125}I]ghrelin from $GHSR_{1a}$ with high and relatively low affinity, respectively (IC_{50} [nM] = 2.5 and 1,300) (Fig. 1*E*).

N8279 Is a Potent Agonist of $GHSR_{1a}$-Mediated $G\alpha_q$ Signaling. $GHSR_{1a}$ primarily couples to $G\alpha_{q/11}$, leading to phospholipase C-β-dependent inositol trisphosphate generation and iCa^{2+} (20). Initial structure-activity relationship screening suggested that the **N8279** precursors **N1965** and **N6164** may exhibit $G\alpha_{q/11}$ bias (*SI Appendix*, Fig. S1*B* and Table S1). To confirm this with the active congener, **N8279** (*SI Appendix*, Fig. S1 *A–C* and Table S2), we performed concentration–response (C/R) analyses in cells stably expressing $GHSR_{1a}$ and an iCa^{2+} reporter (21). The results show that **N8279** is nearly an order of magnitude (8.9-fold) more potent than the endogenous ligand ghrelin and is a full agonist (Fig. 1*F*). **N8279** was only 3.4- and 5.3-fold less potent than the high-affinity, unbiased small molecule agonists L585 and MK-0677, respectively (Fig. 1*F*). Consistent with prior work (26), ghrelin was relatively weak at stimulating iCa^{2+} compared to its $GHSR_{1a}$ binding affinity (Fig. 1 *E* and *F*; Ref. 26). Conversely, the iCa^{2+} half-maximal effective concentration (EC_{50}) of **N8279** was 41-fold more potent than its $GHSR_{1a}$ binding IC_{50} (Fig. 1 *E* and *F*), suggesting possible allosteric activity (26). Only ghrelin and **N8279** each had a Hill slope (h) > 1, suggesting that two or more molecules or $GHSR_{1a}$ binding sites are required for these ligands to elicit full efficacy in this cell system (Fig. 1*F*).

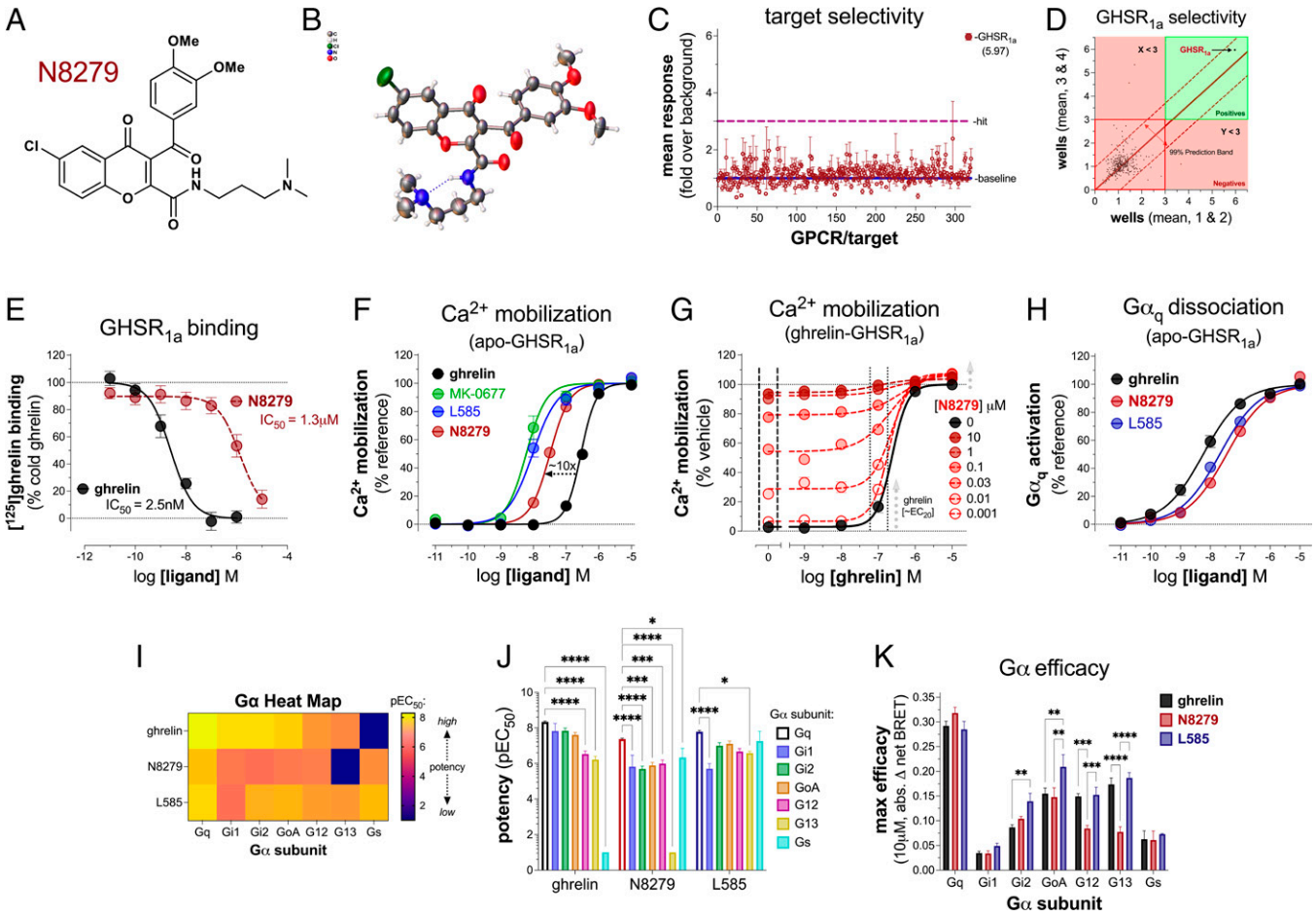

Fig. 1. **N8279** is a potent agonist of $GHSR_{1a}$-mediated $G\alpha_q$ signaling. **N8279** (*A*) 2D structure and (*B*) structure determined by single crystal X-ray diffraction. (*C*) **N8279** (1 μM) selectivity for human $GHSR_{1a}$ plotted versus onefold (blue line) and ≥3-fold (dotted purple line) activity above baseline. (*D*) Linear regression analysis of βarr-based Tango assay results for GPCRome with each point XY corresponding to a distinct receptor and its coordinates defined by X = average of replicates 1 and 2 and Y = average of replicates 3 and 4. (*E*) [^{125}I]ghrelin competition binding in $hGHSR_{1a}^{WT}$-expressing HEK293/T cells (unlabeled ghrelin curve, black; **N8279** curve, red). Data were normalized to vehicle conditions within each experiment and pooled data normalized to the unlabeled (cold) ghrelin *Top* (100%) and *Bottom* (0%). (*F*) iCa^{2+} in $hGHSR_{1a}^{WT}$ and miAeq-expressing HEK293/N cells after treatment with ghrelin (black), MK-0677 (green), L585 (blue), or **N8279** (red). *Bottom* and *Top* parameters were constrained to 0% and 100% of ghrelin (% reference); ghrelin and **N8279** $h > 1$. (*G*) Ghrelin-induced iCa^{2+} with concomitant **N8279** treatment. Data are normalized to the vehicle E_{max} (100%) and the image displays best-fit three- or four-parameter regressions for each condition. (*H*) $G\alpha_q$ dissociation (TRUPATH) in $hGHSR_{1a}^{WT}$-expressing HEK293/T cells. *Bottom* and *Top* parameters were constrained to 0% and 100% of ghrelin (% reference) and the *h* shared ($P > 0.05$). (*I–K*) Ghrelin, **N8279**, and L585 heat map (*I*); yellow—higher potency, blue—lower potency or inactivity; (pEC_{50}) potencies (*J*) and max efficacies (10 μM) (*K*) at different G proteins derived from curves in *SI Appendix*, Fig. S4. Statistical differences are derived from Dunnett's multiple comparisons relative to each ligand's $G\alpha_q$ response. $^*P < 0.05$, $^{**}P < 0.01$, $^{***}P < 0.001$, $^{****}P < 0.0001$. All data represent the mean ± SEM from multiple independent experiments.

The iCa^{2+} evoked by EC_{80} **N8279** (*SI Appendix*, Fig. S3*B*), ghrelin (*SI Appendix*, Fig. S3*C*), or L585 (*SI Appendix*, Fig. S3*D*) was competitively inhibited by the $GHSR_{1a}$ antagonists YIL781 and JMV2959, supporting $GHSR_{1a}$-dependent effects. For each agonist, YIL781 was the more potent inhibitor (*SI Appendix*, Fig. S3 *B–D*). To determine whether **N8279** elicits $GHSR_{1a}$-mediated iCa^{2+} through $G\alpha_{q/11}$ specifically, we tested iCa^{2+} in $G\alpha_{q/11}$ KO and wild-type (WT) cells (27) and confirmed that 10 μM ghrelin-, L585-, and **N8279**-induced iCa^{2+} was abolished (*SI Appendix*, Fig. S3*E*).

We next evaluated the effect of **N8279** on ghrelin-induced iCa^{2+} signaling to test for ago-allosteric activity. Parenthetically, ago-allosteric agonists interact with topographically distinct receptor sites (allosteric) from the endogenous ligand (orthosteric), elicit agonist behavior on their own, and cooperatively act as a positive (PAM), negative (NAM), or silent (SAM) modulator of orthosteric ligand affinity, potency, and/or efficacy (28). As expected, **N8279** displayed intrinsic $GHSR_{1a}$ agonism on its own (Fig. 1*G*, left dashes). At 10 μM, **N8279** produced an ∼3-fold increase in ghrelin's potency but did not reach statistical significance (Fig. 1*G*). **N8279** additively increased ∼EC_{20} ghrelin (100 nM) efficacy in a concentration-dependent manner (Fig. *G*, right dashes/upward arrow) and marginally increased the ghrelin E_{max} (Fig. 1*G*, upward arrow), supporting weak ago-PAM activity (29). To assess reciprocal cooperativity, we tested iCa^{2+} upon concomitant treatment of EC_{25} MK-0677 or EC_{50} ghrelin and an **N8279** C/R. In the presence of these orthosteric agonists, **N8279** was equipotent relative to **N8279** alone; however, the *h* of **N8279** alone ($h > 1$) was reduced to unity ($h = 1$) (*SI Appendix*, Fig. S3*F*). These findings indicate that **N8279** evokes a complete and potent signaling response despite simultaneous occupancy of the $GHSR_{1a}$ orthosteric binding pocket.

To model how **N8279** could co-occupy the monomeric $GHSR_{1a}$ with ghrelin, we employed molecular docking with an NMR-based homology model of the ghrelin-bound $GHSR_{1a}$ (30). Concomitant **N8279** docking to ghrelin (1–17, amino

PHARMACOLOGY

acids)–bound $GHSR_{1a}$ suggests that the propylamine moiety of **N8279** could form a strong ionic bond with a negatively charged ECL2 (Asp191) (*SI Appendix*, Fig. S3*G*). In this pose, **N8279** was found to bind $GHSR_{1a}$ atop ghrelin, enabling ghrelin's N terminus to insert into the deep orthosteric binding pocket and interact with Glu124 in transmembrane domain (TM)-III, consistent with prior models and the proposed agonist-induced activation mechanism of $GHSR_{1a}$ (30, 31). Thus, **N8279** may exhibit state-dependent allosteric $GHSR_{1a}$ binding by anchoring to ECL2.

N8279 Biases $GHSR_{1a}$ Toward $G\alpha_q$ Coupling over Other Gα Subunits. To evaluate the effect of **N8279** on $G\alpha_q$ proximal to the $GHSR_{1a}$, we employed parallel NanoBiT- (32) and bioluminescence resonance energy transfer (BRET, TRUPATH; Ref. 33)–based heterotrimeric G protein subunit dissociation approaches. In both assays, **N8279** was a full agonist for $G\alpha_q$ activation with a potency comparable to that of iCa^{2+} (Fig. 1*H* and *SI Appendix*, Figs. S1*F* and S3*H*). In NanoBiT-$G\alpha_q$ assays, **N8279** and ghrelin potencies were statistically equivalent (*SI Appendix*, Fig. S3*H*). In BRET-$G\alpha_q$ assays, **N8279** was 6.1- and 1.7-fold less potent than ghrelin and L585, respectively (Fig. 1*H*). In contrast to iCa^{2+} assays (Fig. 1*F*), the *h* was <1 for each agonist. These differences may be due to distinct G protein subunit composition/ratios and/or response sensitivities between these assays (see *Materials and Methods*). Notably, ghrelin was ∼30 to 50-fold more potent at activating $G\alpha_q$ proximally than eliciting downstream iCa^{2+} (Fig. 1 *F* and *H* and *SI Appendix*, Fig. S3*H*), consistent with a prior report (26). These findings suggest that in these cell systems, low ghrelin concentrations are sufficient to dissociate the heterotrimeric $G\alpha_q$ complex, whereas high ghrelin concentrations are required to fully engage downstream $GHSR_{1a}$ signaling, as seen with other homodimeric GPCRs (34). Alternatively, ghrelin could elicit $G\alpha_q$-independent signaling that counter regulates iCa^{2+} in this assay. Collectively, these results demonstrate that **N8279** is a potent agonist of $G\alpha_q$ signaling at $GHSR_{1a}$.

In an independent set of experiments, we evaluated **N8279** signaling through other G proteins to compare to $G\alpha_q$. We selectively tested Gα subunits that are expressed highly in midbrain DAergic neurons (35) and/or reported previously to exhibit $GHSR_{1a}$ coupling, including $G\alpha_{sS}$ ($G\alpha_s$), $G\alpha_{i1}$, $G\alpha_{i2}$, $G\alpha_{oA}$, $G\alpha_{12}$, and $G\alpha_{13}$ (19, 23, 36). Relative to $G\alpha_q$, ghrelin potency was statistically equivalent for each $G\alpha_{i/o}$ and was reduced moderately for $G\alpha_{12}$ and $G\alpha_{13}$ (Fig. 1 *I* and *J* and *SI Appendix*, Fig. S4). Ghrelin did not activate $G\alpha_s$, consistent with a prior study (19). L585 displayed a similar profile, except that it had reduced potency at $G\alpha_{i1}$ and only a statistical trend for reduced potency at $G\alpha_{12}$. In contrast, **N8279** potency was significantly reduced to concentrations >1 μM for every Gα (Fig. 1 *I* and *J* and *SI Appendix*, Fig. S4), suggesting bias toward $G\alpha_q$ coupling. Although **N8279** and L585 showed statistically equipotent activation of $G\alpha_s$, their maximal efficacies (10 μM) at $G\alpha_s$ were markedly reduced (Fig. 1*K* and *SI Appendix*, Fig. S4). Moreover, **N8279** maximum efficacy was significantly reduced at $G\alpha_{12/13}$ compared to ghrelin and L585, as well as at $G\alpha_{i2}$ and $G\alpha_{oA}$ compared to L585 (Fig. 1*K* and *SI Appendix*, Fig. S4). For each ligand, maximal efficacy was reduced at every Gα relative to their respective effect on $G\alpha_q$ (Fig. 1*K* and *SI Appendix*, Fig. S4).

Together, the data in Fig. 1 support that **N8279** is a potent $GHSR_{1a}$ agonist with functional selectivity toward $G\alpha_q$. All pharmacological results (IC_{50}, K_i, $logEC_{50}$, E_{max}, *h* ± SEM) and statistical comparisons for Fig. 1 are shown in *SI Appendix*, Table S3.

N8279 Recruits βarr2 to $GHSR_{1a}$ More Weakly than Ghrelin. Having established that **N8279** is a potent activator of $G\alpha_q$ signaling, we next assessed its effect on $GHSR_{1a}$-mediated βarr recruitment first using a NanoBiT-based approach. Cells expressing a fixed ratio of $GHSR_{1a}^{LgBiT}$ and ^{SmBiT}βarr2 were treated with ghrelin, L585, or **N8279**. Here, **N8279** was ∼20-fold less potent than ghrelin, and it approached full agonism (Fig. 2*A*). Conversely, L585 recruited βarr2 with moderately higher potency and equivalent efficacy to ghrelin (Fig. 2*A*), and comparatively, **N8279** was ∼43-fold less potent than L585 in this assay. Thus, **N8279** is a weaker agonist of $GHSR_{1a}$-βarr2 recruitment than ghrelin and L585, supporting that it exhibits functional selectivity toward $G\alpha_q$ over βarr coupling (Fig. 1).

To further test this hypothesis, cells expressing a variable ratio of $GHSR_{1a}^{LgBiT}$ and ^{SmBiT}βarr2 were treated with ghrelin (100 nM) or ∼EC_{80} **N8279** for $G\alpha_q$ signaling (100 to 200 nM; Fig. 1 *F* and *H* and *SI Appendix*, Fig. S3*H*). These analyses revealed that the relative affinity (BiT_d) of βarr2 for $GHSR_{1a}$ was 2- to 2.5-fold weaker in **N8279**-treated cells than in ghrelin-treated cells (Fig. 2*B*, Inset). Furthermore, in competitive binding studies with the ICL2 mutant $GHSR_{1a}^{L149G}$ (Fig. 2*C*), a βarr2-biased receptor (20), the ability of **N8279** to displace [^{125}I]ghrelin was diminished and shifted rightward by ∼10-fold (IC_{50} > 10 μM) relative to $GHSR_{1a}^{WT}$ (Fig. 1*E*). In contrast, the IC_{50} of unlabeled ghrelin for $GHSR_{1a}^{L149G}$ was reduced by only ∼2-fold compared to $GHSR_{1a}^{WT}$ (Figs. 1*E* and 2*C*). A follow-up, BRET-based $GHSR_{1a}^{L149G\text{-}RLucII\text{-}Venus}$βarr2 recruitment assay further supported distinct properties between ghrelin and **N8279** at the βarr-biased $GHSR_{1a}^{L149G}$. While $GHSR_{1a}^{L149G}$ reduced the E_{max} of ghrelin and **N8279** to similar extents (∼35%), the **N8279** potency was reduced by ∼5-fold, whereas the ghrelin potency was reduced by only ∼2-fold relative to $GHSR_{1a}^{WT}$ (Fig. 2*D*). Notably, interassay comparisons revealed that **N8279** was ∼100-fold less potent than ghrelin in BRET-based $GHSR_{1a}^{WT}$-βarr2 recruitment assays (Fig. 2*D*) but only ∼20-fold less potent in NanoBiT-based measurements (Fig. 2*A*). This distinction may be due to variations in $GHSR_{1a}$-βarr2 expression ratios, biosensor interaction kinetics, and/or measurement time, e.g., $GHSR_{1a}$-βarr2 expression ratios (BRET = 1:15 versus NanoBiT = 1:1) and measurement durations (BRET = 60 min versus NanoBiT = 5 min). Nonetheless, these findings together suggest that **N8279** stabilizes $GHSR_{1a}$ conformations that disfavor $GHSR_{1a}$-βarr2 coupling relative to ghrelin and, reciprocally, that $GHSR_{1a}$ conformations preferentially supporting βarr2 coupling ($GHSR_{1a}^{L149G}$) diminish **N8279**-$GHSR_{1a}$ interaction(s).

Next, we assessed whether **N8279**—as an agonist functionally selective for $G\alpha_q$—could behave as a βarr2 antagonist in the presence of ghrelin. We pretreated cells expressing $GHSR_{1a}^{LgBiT}$ and ^{SmBiT}βarr2 with increasing concentrations of **N8279** or the antagonists YIL781 or JMV2959, followed by EC_{80} ghrelin. **N8279** inhibited ghrelin-induced βarr2 recruitment significantly, but incompletely, in a concentration-dependent manner and was 1.7- and 2.9-fold less potent than JMV2959 and YIL781 (Fig. 2*E*). These data suggest that **N8279** stabilizes $GHSR_{1a}$ conformation(s) that weaken βarr2 coupling in both apo- (Fig. 2 *A*, *B*, and *D*) and ghrelin-bound (Fig. 2*E*) receptor states.

N8279 Reduces βarr-Dependent Cellular Responses Relative to Ghrelin. Qualitative microscopy of U2OS cells expressing $GHSR_{1a}$ and $βarr2^{GFP}$ showed minimal response to 100 nM **N8279** and displayed diffusely distributed cytosolic $βarr2^{GFP}$ similar to vehicle-treated cells (Fig. 2*F*). Conversely, 100 nM ghrelin–treated cells exhibited marked accumulation of cytosolic puncta, indicative of robust $βarr2^{GFP}$ translocation and $GHSR_{1a}$ endocytosis/trafficking (Fig. 1*F*). Though ghrelin produced a robust response, the relatively weak response produced by **N8279** in these experiments may reflect differences in engagement with early (e.g., GPCR kinases; Ref. 37) or late molecular mediators of receptor endocytosis and/or endosomal trafficking (21). Thus, we evaluated ligand-induced $GHSR_{1a}$ endocytosis using three independent methods. First, in a

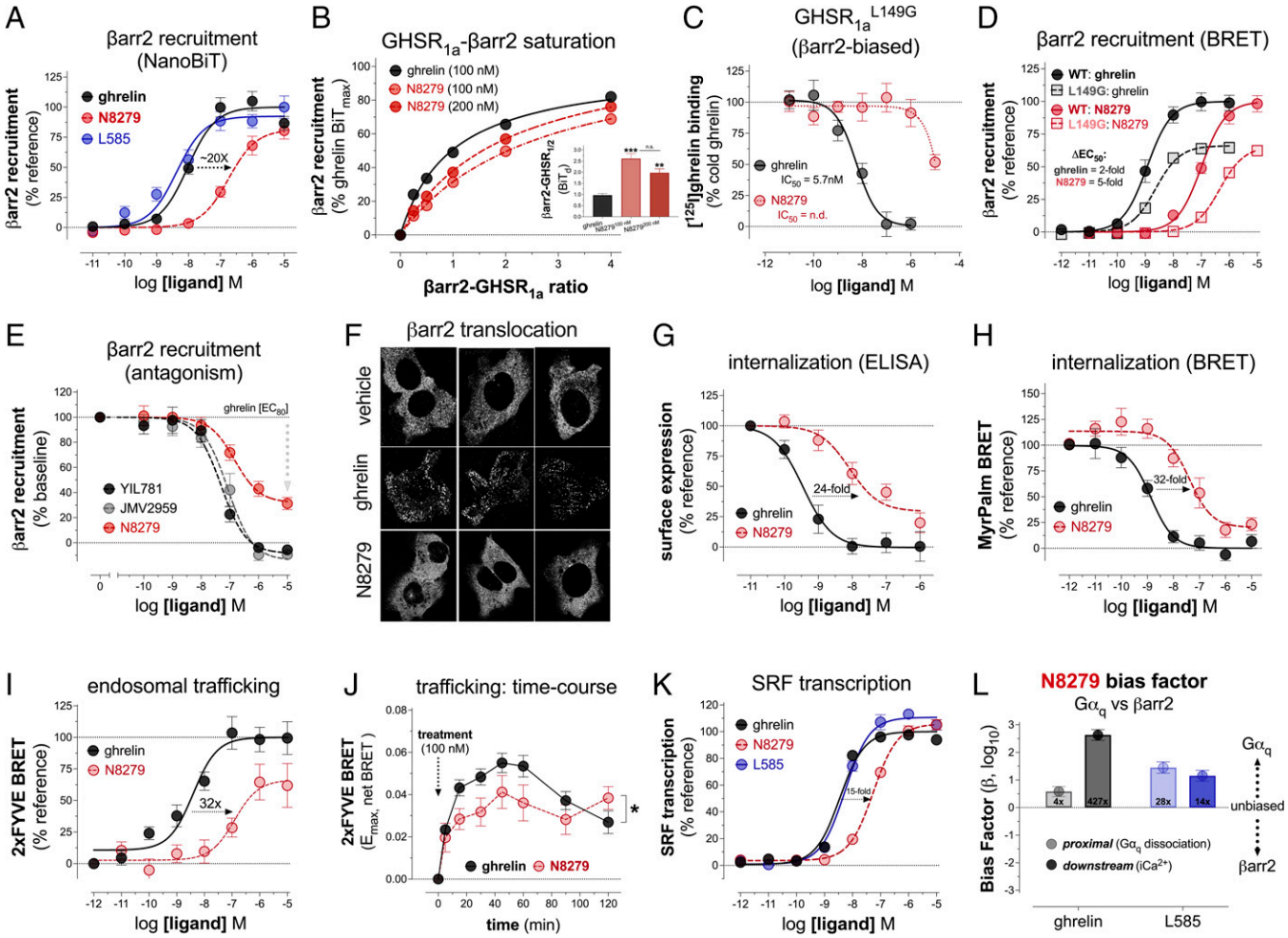

Fig. 2. **N8279** is a weak activator of $GHSR_{1a}$-mediated, βarr2-dependent cellular responses relative to ghrelin. (*A*) Peak ^{SmBiT}βarr2 recruitment (average, 0 to 5 min) to $hGHSR_{1a}^{LgBiT}$ in HEK293/T cells. Data were baseline normalized within each experiment, then to the ghrelin E_{max} (% reference). (*B*) $hGHSR_{1a}^{LgBiT\text{-}SmBiT}$βarr2 saturation after treatment with ghrelin (100 nM, black) or **N8279** (100 nM, light red; 200 nM, dark red). Hyperbola were fit by one-site regression to derive a B_{max} (BiT_{max}) and K_d (BiT_d), then normalized to the ghrelin BiT_{max} (100%). (*B*, *Inset*) Ghrelin and N8279 BiT_d values derived from *B* and analyzed by one-way analysis of variance (ANOVA) followed by Sidak's multiple comparisons. (*C*) [^{125}I]ghrelin competition binding in HEK293/T cells expressing $hGHSR_{1a}^{L149G}$. Data were normalized as in Fig. 1*E*. (*D*) Maximum ^{Venus}βarr2 recruitment (over 60 min) to $hGHSR_{1a}^{WT}$ or $hGHSR_{1a}^{L149G}$ in HEK293/T cells. Data were baseline normalized within each experiment, then the ghrelin-WT E_{max} (% reference). (*E*) EC_{80} ghrelin (40 nM)–induced ^{SmBiT}βarr2 recruitment to $hGHSR_{1a}^{LgBiT}$ after pretreatment (5 min) with YIL781, JMV2959, or **N8279**. The 100% point represents EC_{80} ghrelin alone and the 0% line represents baseline. (*F*) Representative images of vehicle-, ghrelin (100 nM)–, or **N8279** (100 nM)–induced βarr2 translocation (45 min, 37 °C) in U2OS cells expressing $hGHSR_{1a}^{WT}$ and $βarr2^{GFP}$. (*G*) $hGHSR_{1a}^{WT}$ internalization in HEK293/T cells (45 min, 37 °C). Data are expressed as the percentage of $GHSR_{1a}$ expression relative to baseline (100%), and pooled data were normalized to the ghrelin *Top* (100%) and *Bottom* (0%) (% reference). (*H*) bBRET-based $hGHSR_{1a}^{WT\text{-}RLucII}$ internalization in HEK293/T cells with $MyrPalm^{Venus}$. Data represent the average net BRET (60 min) normalized to baseline within each experiment and then to the ghrelin *Top* (100%) and *Bottom* (0%) (% reference). (*I*) bBRET-based $hGHSR_{1a}^{WT\text{-}RLucII}$ trafficking in HEK293/T cells with $2{\times}FYVE^{Venus}$. Data represent the average net BRET (60 min) normalized to the ghrelin E_{max} (% reference). (*J*) $GHSR_{1a}$ trafficking E_{max} over 120 min as derived from *I*. (*K*) SRF-RE–mediated transcription in HEK293/T cells expressing $hGHSR_{1a}^{WT}$. Data were normalized to the ghrelin E_{max} (% reference). (*L*) **N8279** bias factor (RA_i model) with β (log_{10}) quantified using ghrelin (black/gray) or L585 (blue) as reference ligands. All data represent the mean ± SEM from multiple independent experiments. ***$P < 0.001$; **$P < 0.01$; *$P < 0.05$; n.s. (nonsignificant), $P > 0.05$.

quantitative, cell surface enzyme-linked immunosorbent assay (ELISA) approach, both ghrelin and **N8279** stimulated $GHSR_{1a}$ internalization in a concentration-dependent manner (Fig. 2*G*). However, **N8279** internalization potency was reduced by 24-fold, and the efficacy was reduced modestly (~30%) relative to ghrelin (Fig. 2*G*). Second, we employed a bystander BRET (bBRET)–based plasma membrane sensor, $MyrPalm^{Venus}$ (38), and found that **N8279**-induced $GHSR_{1a}$ internalization (over 60 min) potency was reduced by 32-fold and efficacy was attenuated by ~20% relative to ghrelin (Fig. 2*H*). Last, the bBRET-based sensor for early endosomes (21, 39), $2{\times}FYVE^{Venus}$ (40), showed that **N8279**-induced $GHSR_{1a}$ endosomal transit was 32-fold less potent and less efficacious (~35%) than ghrelin over 60 min posttreatment (Fig. 2*I*). Temporal analyses revealed that **N8279**-stimulated $GHSR_{1a}$ endosomal trafficking occurred on a time course similar to ghrelin, albeit with reduced efficacy across the entire 120-min measurement (Fig. 2*J*).

βarr2 is required for $GHSR_{1a}$-mediated RhoA GTPase/ROCK signaling (41), leading to transcriptional activation and cytoskeletal rearrangement by induction of actin polymerization (20). To test whether **N8279** affects these processes, we utilized the RhoA-dependent transcriptional reporter serum response factor response element (SRF-RE) (20). Here, **N8279** was a full agonist with mildly increased maximal efficacy relative to ghrelin (Fig. 2*K*). However, **N8279** potency was reduced ~10- to 15-fold relative to L585 and ghrelin, respectively. The

enhanced efficacy of **N8279** in these assays compared to Fig. 2 *G–J* could be a time-dependent effect, in part, due to the 6-h treatment duration (see *Materials and Methods*) and/or the partial contribution(s) of $G\alpha_{12/13}$ or especially MAPK/ERK signaling to SRF transcription (20).

To quantitatively assess **N8279** bias between the $G\alpha_q$ and βarr2 (Fig. 2*A*) pathways, we used the intrinsic relative activities (RA_i) model as described previously (42). Relative to ghrelin, **N8279** had a proximal ($G\alpha_q$ dissociation, Fig. 1*H*) bias factor (β) of 0.59 (~4-fold) and a downstream (iCa^{2+}, Fig. 1*F*) β of 2.63 (~427-fold) relative to βarr2 recruitment (NanoBiT, Fig. 2*A*) (Fig. 2 *L*, *Left*). Relative to L585, **N8279** had a proximal β of 1.45 (~28-fold) and a downstream β of 1.15 (~14-fold) (Fig. 2 *L*, *Right*). Notably, assay-standardized bias calculations (i.e., $G\alpha_q$-βarr2 BRET versus $G\alpha_q$-βarr2 NanoBiT) using ghrelin as a reference ligand showed that **N8279** had a proximal β of 1.16 (~14-fold) and 1.36 (~23-fold) when employing paired BRET-$G\alpha_q$/BRET-βarr2 or NanoBiT-$G\alpha_q$/NanoBiT-βarr2 assays, respectively (*SI Appendix*, Fig. S5). Ultimately, these analyses together support that **N8279** is a G protein–biased agonist of both proximal and downstream $GHSR_{1a}$-$G\alpha_q$ signaling.

Collectively, the data in Fig. 2 support that **N8279** is a weak agonist of $GHSR_{1a}$-mediated, βarr-dependent signaling relative to ghrelin, and thus, **N8279** is a G protein–biased $GHSR_{1a}$ agonist. All pharmacological results and statistical comparisons for Fig. 1 are shown in *SI Appendix*, Table S4.

$GHSR_{1a}$ Mutagenesis and Molecular Docking Suggest an ECD-Dependent, Extended Binding Mode of N8279. We next evaluated whether determinants outside the orthosteric binding pocket are required for **N8279** signaling by first using a naturally occurring variant, $GHSR_{1a}^{A204E}$ (Fig. 3*A*). Substitution of glutamic acid at this ECL2 site abolishes constitutive activity and causes short stature in humans (43). However, the $GHSR_{1a}^{A204E}$ mutation does not appreciably affect ghrelin binding (affinity) or ghrelin-induced $G\alpha_q$ signaling (potency) (43, 44), supporting that it lies outside the orthosteric binding pocket.

Consistent with prior studies (43, 44), $GHSR_{1a}^{A204E}$ showed no basal iCa^{2+} activity (Fig. 3 *B* and *C*); surface expression was reduced by ~50% (*SI Appendix*, Fig. S6*A*); it had minimal-to-no effect on ghrelin-stimulated $G\alpha_q$ dissociation and iCa^{2+} (Fig. 3 *B* and *C*); and ghrelin-stimulated βarr2 recruitment efficacy, but not potency, was reduced (Fig. 3*D*; Ref. 44). In contrast, **N8279**-induced iCa^{2+} potency was reduced by 6.5-fold, while full agonism was retained (Fig. 3*E*). Furthermore, **N8279**-induced $G\alpha_q$ dissociation signaling was reduced dramatically such that the C/R curve did not saturate, supporting that the **N8279** potency is blunted by >20-fold and the maximal efficacy decreased by ~45% (Fig. 3*F*). The effect magnitude discrepancy between measurements of iCa^{2+} and Gα dissociation likely reflects signal amplification differences between the assays. **N8279**-induced βarr2 recruitment potency at $GHSR_{1a}^{A204E}$ was similarly diminished (>20-fold) and did not reach saturation, with a maximal efficacy comparable to ghrelin (~35%; Fig. 3*G*). Thus, relative to ghrelin, **N8279** signaling requires distinct ECL2 sites and/or ECD-dependent conformational states.

Next, we used the NMR-based homology model of the ghrelin-bound $GHSR_{1a}$ (*SI Appendix*, Fig. S3*G*) (30) to simulate **N8279**-$GHSR_{1a}$ binding. We deprioritized the antagonist-bound $GHSR_{1a}$ crystal structure (45) (Fig. 3*H* and *SI Appendix*, Fig. S7) because it better models the inactive $GHSR_{1a}$ conformation (45). Docking **N8279** with ghrelin removed discloses two potential binding modes for **N8279** within the apo-$GHSR_{1a}$ (Fig. 3*I*). Both modes display strong ionic interactions between **N8279**'s propylamine moiety and specific acidic (negatively charged) $GHSR_{1a}$ residues. In one mode (Fig. 3*J*, red), **N8279**'s terminal tertiary amine group forms a salt bridge with the conserved TMIII residue Glu124, located within the deep transmembrane pocket ($GHSR_{1a}^{DTP}$). In the second mode (Fig. 3*K*, blue), **N8279**'s propylamine moiety forms a salt bridge with Asp99 toward the top of TMII, enabling an extended binding mode into the ECD ($GHSR_{1a}^{ECD}$) or extracellular vestibule, including the extracellular end of TMVII and ECL2. Notably, the superficial residue Asp99 is too distant from Glu124 (12.7 Å) for **N8279** to interact with both sites simultaneously (Fig. 3*I*). Thus, both docking models suggest that **N8279** binds $GHSR_{1a}$ via ionic interactions with spatially distinct anchor residues. In $GHSR_{1a}^{ECD}$, **N8279**'s methoxy-aromatic and amide moieties form hydrogen bonds with or adjacent to potential allosteric sites based on prior mutagenesis by others (44, 46), including Asn305 on TMVII and Glu197, Arg199, or Pro200 in ECL2 (Fig. 3*K*). Here, **N8279**'s amide group forms an H^+ bond with Cys198, a highly conserved GPCR residue that constrains ECL2 flexibility (Fig. 3*K*) (47). Notably, **N8279** had comparable docking scores within both potential binding pockets: $GHSR_{1a}^{ECD}$ (−6.732) and $GHSR_{1a}^{DTP}$ (−6.767) (Fig. 3 *J* and *K*).

To test our model, we made point mutations to predicted **N8279**-$GHSR_{1a}$ interaction sites or residue clusters (Fig. 3*L*). Given the evidence for critical ECL2-dependent contributions to **N8279** signaling (Fig. 3 *E–G*), as well as the absolute requirement of the $GHSR_{1a}^{DTP}$ anchor residue, Glu124, for $GHSR_{1a}$ function/activation (30, 45, 46), we prioritized the $GHSR_{1a}^{ECD}$-**N8279** docking model for mutagenesis. Alanine substitution to the putative anchor residue Asp99 (Fig. 3*K*, blue) abolished **N8279** signaling (Fig. 3 *M* and *N* and *SI Appendix*, Fig. S6 *B* and *C*). However, the surface expression of this was reduced markedly (*SI Appendix*, Fig. S6*A*), as shown previously (45). Mutations were not made to $Cys198^{ECL2}$ (Fig. 3*K*, light blue) because it precludes GPCR stability and ligand binding (48). Instead, we made alanine substitutions to three adjacent, putative allosteric (44, 46) and/or structurally integral (30) ECL2 residues: Glu197, Arg199, and Pro200 (Fig. 3*K*, blue). We also made an alanine substitution to Asn305, which is located at the extracellular end of TMVII (Fig. 3*K*, blue) and thus is considered within the ECD.

Relative to the WT receptor, the surface expression of the $GHSR_{1a}^{E197A}$ was reduced moderately, the $GHSR_{1a}^{R199A}$ was comparable, and the $GHSR_{1a}^{P200A}$ was increased mildly (*SI Appendix*, Fig. S6*A*). **N8279** potency at the $GHSR_{1a}^{E197A}$ was diminished by ~3- to 10-fold in iCa^{2+} and $G\alpha_q$ dissociation, respectively, whereas the **N8279** E_{max} was reduced in iCa^{2+}, but not $G\alpha_q$ dissociation assays (Fig. 3 *M* and *N* and *SI Appendix*, Fig. S6 *B* and *C*). The $GHSR_{1a}^{R199A}$ mutation did not affect **N8279** potency in either assay, but its E_{max} was reduced mildly in iCa^{2+} assays (Fig. 3 *M* and *N* and *SI Appendix*, Fig. S6 *B* and *C*). **N8279** potency and E_{max} were reduced dramatically at the $GHSR_{1a}^{P200A}$ in both $G\alpha_q$ dissociation and iCa^{2+} assays (Fig. 3 *M* and *N* and *SI Appendix*, Fig. S6 *B* and *C*). Grouped analysis of the **N8279** potency and E_{max} at $GHSR_{1a}^{A204E}$ relative to other mutants supported markedly decreased **N8279**-induced $G\alpha_q$ signaling at this ECL2 residue (Fig. 3 *E*, *F*, *M*, and *N*), despite its location being outside of the putative $GHSR_{1a}^{ECD}$ binding pocket (Fig. 3 *A* and *K*). Alanine substitution to Asn305 did not affect surface expression relative to the WT receptor (*SI Appendix*, Fig. S6*A*), although **N8279**-$G\alpha_q$ dissociation was reduced dramatically and **N8279**-iCa^{2+} potency was reduced moderately (6.5-fold). Surprisingly, the **N8279**-iCa^{2+} E_{max} was elevated at $GHSR_{1a}^{N305A}$ (Fig. 3 *M* and *N* and *SI Appendix*, Fig. S6 *B* and *C*). Generally, any observed differences between **N8279**-induced $G\alpha_q$ dissociation or iCa^{2+} at these mutants could be due to distinctions in assay kinetics or signal amplification, GPCR-transducer expression ratios, and/or the involvement of other transducers (e.g., $G\alpha_{11}$, $G\alpha_{i/o}$, $G\beta\gamma$) in the iCa^{2+} response (49, 50). Together, these mutagenesis findings support that **N8279** signaling requires $GHSR_{1a}$ sites within and/

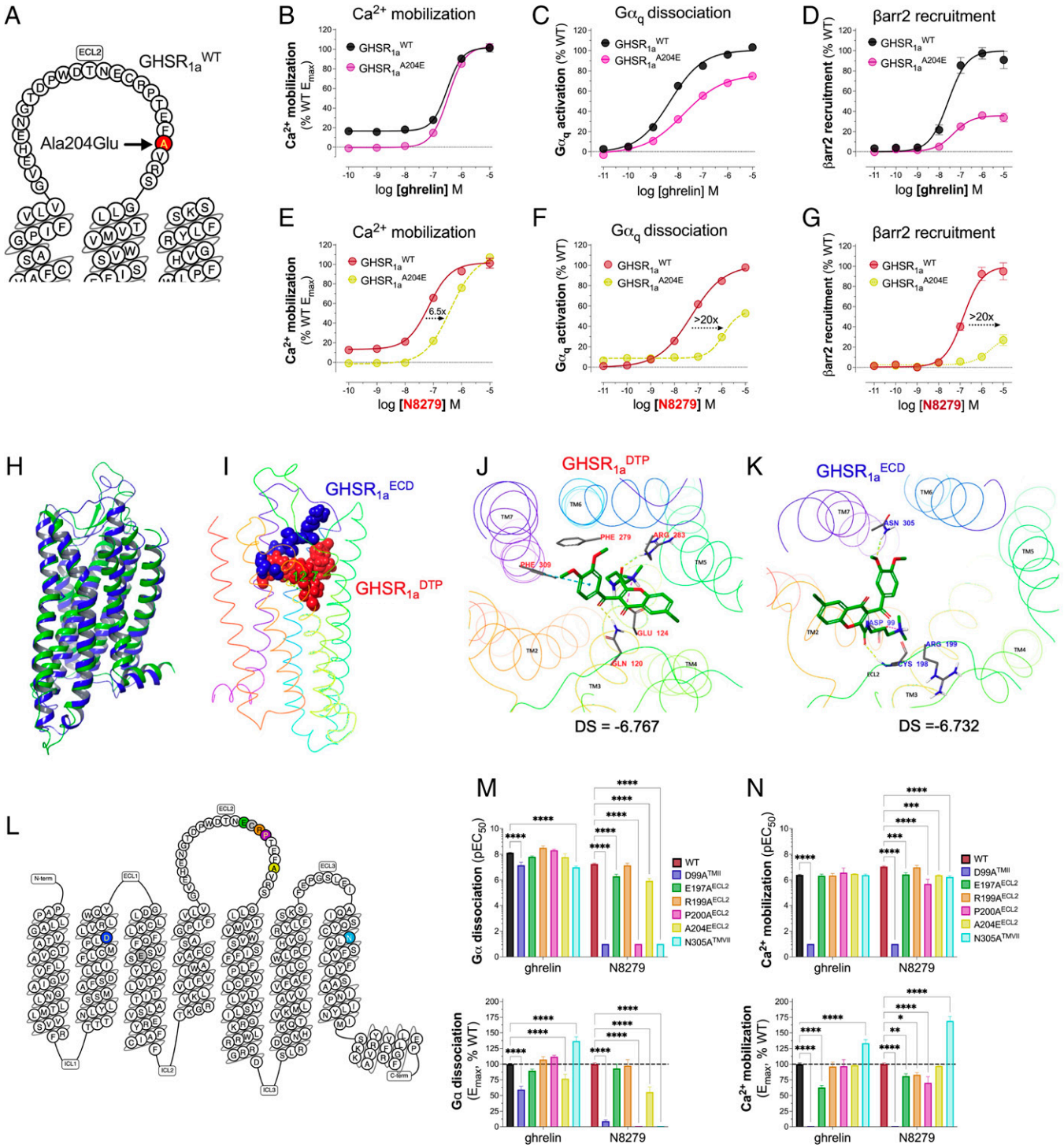

Fig. 3. **N8279** requires receptor sites and/or conformational states driven by the $GHSR_{1a}$ ECD that are distinct from ghrelin. (*A*) Amino acid snake plot of the $hGHSR_{1a}^{WT}$ highlighting $Ala204^{ECL2}$ (red) and the Ala204Glu mutation. Ghrelin-induced (*B*) iCa^{2+}, (*C*) TRUPATH G_q dissociation, and (*D*) NanoBiT βarr2 recruitment at $hGHSR_{1a}^{WT}$ (black) or $hGHSR_{1a}^{A204E}$ (purple). **N8279**-induced (*E*) iCa^{2+}, (*F*) TRUPATH $G\alpha_q$ dissociation, and (*G*) NanoBiT βarr2 recruitment at $hGHSR_{1a}^{WT}$ (red) or $hGHSR_{1a}^{A204E}$ (yellow). All data are normalized to the $GHSR_{1a}^{WT}$ E_{max}. $G\alpha_q$ dissociation and βarr2 recruitment assays are also baseline normalized. (*H*) Superimposition of the ghrelin-bound model structure (blue) with the antagonist-bound X-ray crystal structure (6KO5, green). (*I*) Proposed $GHSR_{1a}^{DTP}$ (red) and $GHSR_{1a}^{ECD}$ (blue) binding pockets in the ghrelin-bound model. Gln120, Glu124, Phe279, Arg283, and Phe309 constitute the canonical orthosteric $GHSR_{1a}^{DTP}$ pocket; mutations to these residues cause significant loss of ghrelin and orthosteric agonist efficacy (46). Asp99, Cys198, and Asn305 constitute predicted interaction sites within the $GHSR_{1a}^{ECD}$ binding pocket of the ghrelin-bound model. (*J*) **N8279** docking pose (green) in $GHSR_{1a}^{DTP}$. (*K*) **N8279** docking pose (green) in $GHSR_{1a}^{ECD}$. Dash lines indicate hydrogen bonds (yellow), ionic interactions (pink) and π–π stacking interactions (turquoise), or halogen bonds (purple). (*L*) Snake plot of $hGHSR_{1a}^{WT}$ with experimentally mutated residues: D99A (blue), E197A (green), R199A (orange), P200A (purple), A204E (yellow), N305A (teal), and Glu124 and Cys198 (gray, mutations not made). (*M*) Ghrelin and **N8279** $G\alpha_q$ dissociation (TRUPATH) and (*N*) iCa^{2+} pEC_{50} and E_{max} at $GHSR_{1a}$ mutants shown in *L*, derived from *SI Appendix*, Fig. S6. All data represent the mean ± SEM from multiple independent experiments.

or conformational states determined by the ECD, especially in ECL2.

For comparison, we evaluated ghrelin-stimulated $G\alpha_q$ dissociation and iCa^{2+} at each $GHSR_{1a}^{ECD}$ mutant. Ghrelin signaling was reduced markedly at $GHSR_{1a}^{D99A}$ in both assays (Fig. 3 *M* and *N* and *SI Appendix*, Fig. S6 *D* and *E*), supporting previous findings (45). However, ghrelin potency at the $GHSR_{1a}^{D99A}$ was similar to $GHSR_{1a}^{WT}$ in $G\alpha_q$ dissociation assays (Fig. 3*M* and *SI Appendix*, Fig. S6*D*). Mutations to Glu197, Arg199, or Pro200 did not significantly affect ghrelin-stimulated $G\alpha_q$ dissociation or iCa^{2+} potency (Fig. 3 *M* and *N* and *SI Appendix*, Fig. S6 *D* and *E*), consistent with prior findings (44, 46). Ghrelin's E_{max} was unaffected at $GHSR_{1a}^{R199A}$ and $GHSR_{1a}^{P200A}$, but it was reduced moderately at $GHSR_{1a}^{E197A}$ in iCa^{2+} assays (Fig. 3 *M* and *N* and *SI Appendix*, Fig. S6 *D* and *E*), consistent with its reduced expression (*SI Appendix*, Fig. S6*A*). Furthermore, grouped analyses (derived from Fig. 3 *B* and *C*) supported that ghrelin potency is unaffected at the $GHSR_{1a}^{A204E}$ mutant and its E_{max} is decreased only in $G\alpha_q$ dissociation assays (Fig. 3 *M* and *N*), consistent with reduced expression of this mutant (*SI Appendix*, Fig. S6*A*). Ghrelin-$G\alpha_q$ dissociation potency was reduced at $GHSR_{1a}^{N305A}$, albeit to a much lesser extent than **N8279** (Fig. 3*M* and *SI Appendix*, Fig. S6 *B* and *D*). Nonetheless, ghrelin-iCa^{2+} potency was not significantly affected by the N305A mutation (Fig. 3*N* and *SI Appendix*, Fig. S6*E*). The ghrelin E_{max} at $GHSR_{1a}^{N305A}$ was increased in both assays (Fig. 3 *M* and *N* and *SI Appendix*, Fig. S6 *D* and *E*), similar to that seen for **N8279**-induced iCa^{2+} (Fig. 3*N* and *SI Appendix*, Fig. S6*C*). Collectively, these findings demonstrate that Glu197, Pro200, Ala204, and, in part, Asn305 are critical and specific $GHSR_{1a}^{ECD}$ sites for **N8279** relative to ghrelin.

Collectively, the data in Fig. 3 support that **N8279** signaling requires molecular determinants within $GHSR_{1a}^{ECD}$ and particularly ECL2. All pharmacological results and statistical comparisons for Fig. 1 are shown in *SI Appendix*, Table S5.

N8279 Is Brain-Penetrant and Attenuates DA-Driven Behavior. Pharmacokinetic studies with intravenous (IV; 1 mg/kg), oral gavage (PO; 5 mg/kg), and intraperitoneal (IP; 5 mg/kg) administration in C57BL/6 mice reveal a PO bioavailability of 7% and IP bioavailability of 27% (*SI Appendix*, Fig. S8 and Table S6). Significantly, IP administration of **N8279** (5 mg/kg) delivered pharmacologically relevant levels (~200 nM) in brain within 15 min, reaching peak concentrations (C_{max}) of 259 nM at 2 h, followed by a slow decline and elimination by 24 h (Fig. 4*A* and *SI Appendix*, Fig. S8 and Table S6). In the brain, **N8279** has a half-life ($t_{1/2}$) of 6.6 to 11 h after IP and PO administration, maintaining levels above its $G\alpha_q/iCa^{2+}$ EC_{50} (~35 nM, Fig. 1 *F* and *H*) for an extended period (>7 h) with a brain/plasma ratio for **N8279** (IP) in the range of 0.6 to 0.9:1 (Fig. 4*A* and *SI Appendix*, Fig. S8 and Table S6). In summary, **N8279** achieves rapid, sustained, and pharmacologically relevant concentrations in mouse brain following systemic administration.

To evaluate the effect of **N8279** on DA-modulated behavior in vivo, we first used DAT KO mice, which have constitutively elevated extracellular DA levels and consequently spontaneous hyperactivity in a novel open field (51). After a 30-min acclimation period, male and female DAT KO mice were administered vehicle or pharmacologically relevant, brain-penetrant doses of **N8279** (Fig. 4*A*; 2.5, 5, or 10 mg/kg, IP), and returned to the open field with locomotion monitored for an additional 120 min. Each dose of **N8279** reduced overall hyperlocomotion in DAT KO mice relative to vehicle controls (Fig. 4 *B* and *C*). Parallel control experiments with inbred male and female C57BL/6J mice indicated that **N8279** does not affect novelty-induced open-field locomotion (*SI Appendix*, Fig. S9).

We next assessed cocaine-induced behavioral sensitization in male and female C57BL/6J mice following subchronic (8-d) administration of the vehicle or **N8279** (5 mg/kg, IP) in the home cage. Subsequently, mice were given the same treatments, and this was followed with injection (IP) of vehicle or cocaine (20 mg/kg) in the open field once a day for 5 consecutive days (Fig. 4 *D*, *Left*). A 5-d hiatus (washout) was imposed, and behavioral sensitization was assessed the next day by giving (IP) vehicle or cocaine (challenge). The cumulative results showed that postinjection locomotor activities were low in the **N8279** + vehicle group and were significantly reduced from the cocaine-treated mice across all days (Fig. 4*D*). By comparison, motor activities were stimulated acutely (day 1) to similar extents in the vehicle + cocaine and **N8279** + cocaine mice (Fig. 4 *D*, *Right*). Locomotion was increased from day 1 though each day to day 5 in the vehicle + cocaine group, whereas significantly enhanced activity was observed only on day 5 in the **N8279** + cocaine mice. Moreover, at challenge (day 11), locomotor activity was augmented relative to day 1 in the vehicle + cocaine mice, whereby no change in activity was evident in the **N8279** + cocaine mice. Thus, **N8279** both delayed the appearance of sensitization across days and abrogated the expression of sensitization following washout (challenge, day 11).

Collectively, these results indicate that pharmacologically relevant and brain-penetrant levels of **N8279** ameliorate aberrant DA-mediated behavior in two mouse models of persistently disrupted DA homeostasis.

Discussion

In this study, we disclose a chemotype of small molecule $GHSR_{1a}$ modulators with functional selectivity toward $G\alpha_q$ signaling. Our results support that the lead compound from this chemical series, **N8279** (NCATS-SM8864), stabilizes conformational states that drive the apo- and ghrelin-bound $GHSR_{1a}$ toward $G\alpha_q$ coupling over other G proteins and βarr-dependent cellular responses. Importantly, **N8279** has excellent brain penetrance and exhibits salutary effects on DA-induced behavior in both genetic and pharmacological mouse models of disrupted DA homeostasis.

Collectively, our findings indicate that **N8279**-induced $GHSR_{1a}$ signaling originates, at least in part, from an extended binding mode into the extracellular vestibule and/or conformational constraints imposed by the $GHSR_{1a}^{ECD}$, especially ECL2. This notion is supported most strongly by significantly reduced **N8279** potency upon mutation of specific ECL2 residues, including Ala204, Pro200, and to a lesser extent Glu197. Critically, these effects are distinct from the endogenous $GHSR_{1a}$ ligand, ghrelin. Although **N8279** is not predicted to interact directly with these residues in our in silico models, they are adjacent or proximal to predicted interaction sites within our $GHSR_{1a}^{ECD}$ binding pocket model. Thus, these mutations may result in $GHSR_{1a}$ conformation(s) that are less accessible for **N8279** binding and/or less capable of stabilizing a signaling-competent **N8279**-$GHSR_{1a}$ complex via perturbation of the ECD structure and/or local disruption(s) to proximal interaction sites. Together, these findings suggest that **N8279** signaling at the apo-$GHSR_{1a}$ is most likely mediated by a bitopic, extended binding mode that is conformationally dependent upon the $GHSR_{1a}^{ECD}$. Additionally, **N8279**-$GHSR_{1a}^{ECD}$ interaction(s) may be state dependent, given that concomitant docking of **N8279** and ghrelin peptide (1–17, amino acids) (30) predicts a strong ionic interaction of **N8279** with ECL2 when at the ghrelin-occupied $GHSR_{1a}$ (*SI Appendix*, Fig. S3*G*). Pharmacologically, these binding properties may contribute to **N8279**'s ability to modestly enhance, or at least noncompetitively retain, $G\alpha_q$ signaling efficacy at the ghrelin-bound $GHSR_{1a}$ (Fig. 1*G*; *SI Appendix*, Fig. S3*F*). Alternatively, these effects could arise from asymmetric interactions between ghrelin, **N8279**, and $GHSR_{1a}$ homodimers within allosteric and/or

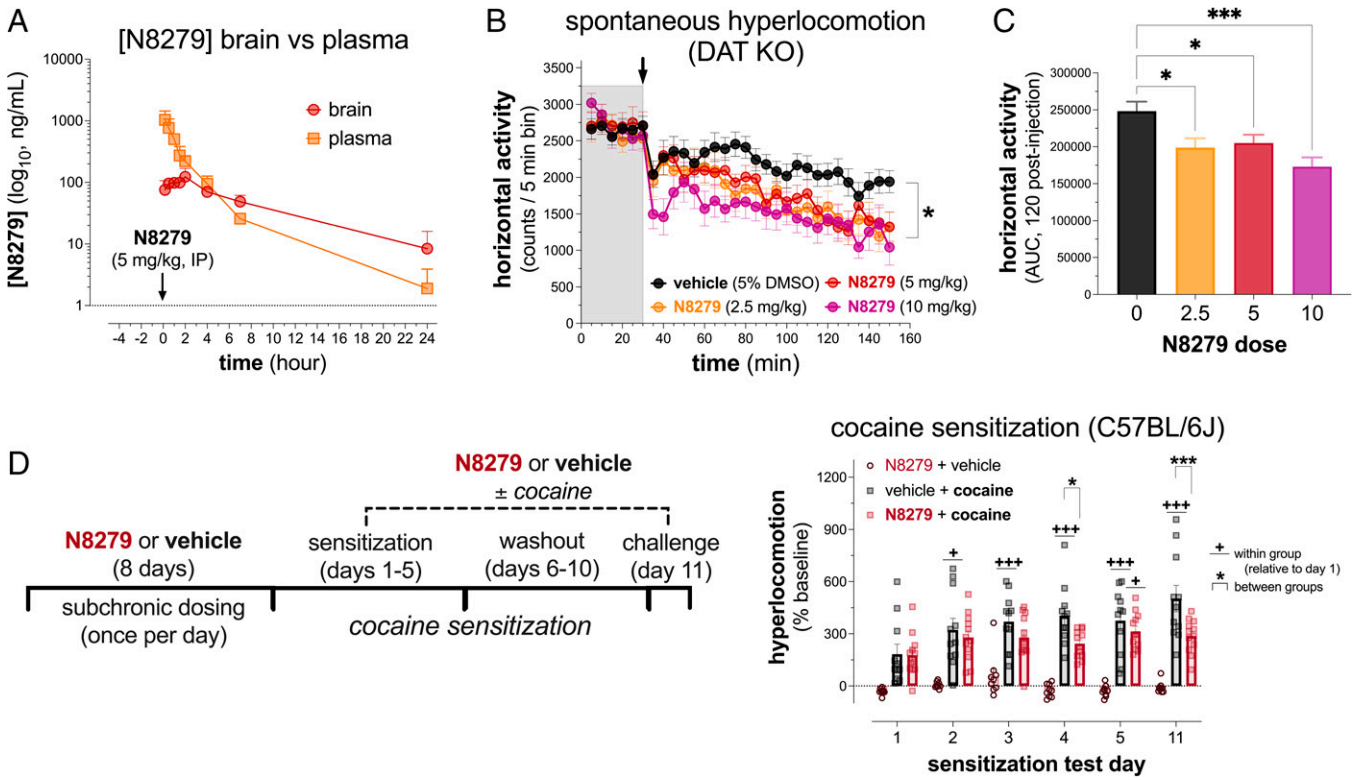

Fig. 4. **N8279** is brain-penetrant and attenuates aberrant DAergic behavior in mice. (*A*) Analysis of brain (red) and plasma [**N8279**] (orange) over 24 h in C57BL/6 mice treated with **N8279** (5 mg/kg, IP). **N8279** C_{max} at ~2 h = 123 ng/mL (259 nM). **N8279** (IP) brain half-life ($t_{1/2}$) = 6.6 h, plasma $t_{1/2}$ = 3.8 h. (*B*) Spontaneous hyperlocomotion in DAT KO mice. 30 min (gray box) acclimation prior to injection (black arrow) of **N8279** (2.5, 5, or 10 mg/kg, IP) or vehicle (5% DMSO, saline). Horizontal locomotion was monitored for 120 min postinjection, and beam breaks were collected in 5 min bins. Results are presented as mean ± SEM. **N8279**-treated DAT KO mice had reduced locomotion relative to vehicle-treated controls. Postinjection, repeated measures ANOVA (RMANOVA), time: [$F(7.6,411.8) = 14.7$, $P < 0.0001$], dose: [$F(3,54) = 3.4$, $P = 0.022$], time × dose interaction: [$F(69,1242) = 1.2$, $P = 0.118$]. No baseline differences were detected between groups. Baseline RMANOVA, time: [$F(2.4,131.0) = 3.0$, $P = 0.039$], dose: [$F(3,54) = 0.06$, $P = 0.979$], time × dose interaction: [$F(15,270) = 1.4$, $P = 0.141$]. n = 12 to 20 mice per group. (*C*) One-way ANOVA for total area under the curve (AUC, 35 to 150 min) derived from *B*. Treatment: [$F(3,55) = 6.50$, $P = 0.0008$]. Dunnett's multiple comparisons revealed an effect of 2.5, 5, and 10 mg/kg **N8279** relative to vehicle control (0 mg/kg). *$P < 0.05$, ***$P < 0.001$ versus vehicle. (*D*) Cocaine-induced behavioral sensitization in C57BL6/J mice: experimental design (*Left*) and locomotion (*Right*). Postinjection results are presented as percentage of baseline activities because locomotion was low in the **N8279** + vehicle group on all days. Within-group analyses (significance denoted by $^{+}$) relative to day 1 showed that the vehicle + cocaine group had increased locomotion on days 2 to 5 and day 11, whereas the **N8279** + cocaine group had increased locomotion only on day 5. Between-group comparisons (significance denoted by *) showed that cocaine-induced sensitization was higher on day 4 and on challenge day 11 in the vehicle + cocaine compared to the **N8279** + cocaine group. RMANOVA: day [$F(5,145) = 8.797$, $P < 0.001$], treatment [$F(2,29) = 32,523$, $P < 0.001$], day × treatment [$F(10,145) = 3.215$, $P < 0.001$]. *$^{/+}P < 0.05$, ***$^{/+++}P < 0.001$. n = 9 to 12 mice/group.

orthosteric binding pockets. This notion is consistent with ghrelin- and **N8279**-induced iCa^{2+} exhibiting an $h > 1$ at the apo-$GHSR_{1a}$ (Fig. 1*E*) and **N8279** having an h of unity at the orthosteric agonist-bound $GHSR_{1a}$ (Fig. 1*F*; *SI Appendix*, Fig. S3*F*). Indeed, $GHSR_{1a}$ homodimerizes (52) and ago-allosteric $GHSR_{1a}$ agonists (e.g., L-692,429) elicit similar effects to **N8279** via bitopic or bimodal state-dependent interaction(s) with the "allosteric" or "orthosteric" protomers of the $GHSR_{1a}$ dimer (26).

Our functional evidence supports the notion that **N8279** stabilizes a conformation favoring the $G\alpha_q$-bound conformation of $GHSR_{1a}$ over other transducers ($G\alpha_{i/o}$, $G\alpha_{12/13}$, and βarr2) relative to ghrelin (Figs. 1 and 2). Conversely, **N8279** displacement of ghrelin binding is blunted at the βarr-biased ICL2 variant, $GHSR_{1a}^{L149G}$, suggesting that the βarr2-coupled $GHSR_{1a}$ renders **N8279** binding at the extracellular face of the receptor less accessible (Fig. 2*C*). Thus, **N8279** pretreatment-induced partial $GHSR_{1a}^{WT}$-βarr2 antagonism may depend on kinetic and/or allosteric mechanism(s). Together, these observations of bidirectional allostery are consistent with the principle of reciprocity underlying ligand–GPCR–transducer and allosteric coupling (i.e., ternary complex model) (53, 54). Indeed, ECL2 is an established determinant of $GHSR_{1a}$ (44) and, more generally, GPCR bias (55, 56). Several biased ligands elicit their effects through extended binding modes involving the cognate GPCR's ECD (especially ECL2), whereby superficial ligand–receptor interactions preferentially stabilize conformations that allosterically propagate to the intracellular receptor face to influence transducer coupling and thereby functional selectivity (57). Some examples of these biased ligand–GPCR pairs include the dopamine D2 receptor (D_2R) (55), the serotonin 2B ($5\text{-}HT_{2B}R$) (58, 59), the muscarinic type 2 (M_2R) (60, 61), the β-adrenergic receptors (β_1AR, β_2AR) (62), and the glucagon-like peptide-1 (GLP-1) receptor (63). Notably, $GHSR_{1a}$-containing tissues likely express different levels of signaling proteins (e.g., Gα subunits, GRKs); thus, "system bias" (64, 65) may be expected (Figs. 1 and 2) to play a significant role in determining **N8279**-induced $GHSR_{1a}$ functional selectivity in vivo.

Pharmacokinetic studies indicate that **N8279** was able to sustain biologically relevant levels in brain for extended periods of time following IP administration of a low dose (5 mg/kg). Critically, in vivo efficacy studies revealed that acute administration of **N8279** at pharmacologically relevant doses attenuated hyperlocomotion in both genetic and pharmacological models of hyperDAergia, recapitulating effects achieved by $GHSR_{1a}$

antagonists (22, 66, 67). Previously, we reported that the antagonist YIL781 reduced hyperlocomotion in cocaine-sensitized WT but not DA neuron–specific βarr2 KO mice (22), suggesting that βarr2 inhibition was required for $GHSR_{1a}$ antagonists to blunt cocaine-induced neuroadaptations. Additionally, $GHSR_{1a}$-induced βarr signaling and, more generally, $G\alpha_{12/13}$ signaling (68, 69) are required for RhoA-dependent actin remodeling—a process integral to neuroplasticity in DA neurons (70, 71). Together, these prior findings suggest that βarr2 might be necessary for the proaddictive effects of $GHSR_{1a}$ activation, particularly during DA plasticity–dependent reward learning (e.g., behavioral sensitization). Here, we show that **N8279** reduced novelty-related hyperlocomotion in DAT KO but not in inbred C57BL6/J mice (Fig. 3 *B* and *C*) and depressed behavioral sensitization in cocaine-sensitized C57BL/6J mice. Thus, it appears that reductions in $GHSR_{1a}$-βarr2 signaling may preferentially blunt the development and/or expression of behaviors mediated by sensitized neurocircuits (e.g., mesolimbic, nigrostriatal) that have undergone DA-dependent plasticity, whereas $GHSR_{1a}$ regulation of metabolic homeostasis (e.g., feeding, glucose/insulin homeostasis, growth hormone secretion) and DA cell neuroprotection are generally considered G protein mediated (9, 23, 72, 73). Thus, an agonist functionally selective for $G\alpha_q$ should bias $GHSR_{1a}$ away from βarr or alternative Gα signaling and thus may retain the antiaddictive effects of $GHSR_{1a}$ antagonists while preserving, normalizing, or augmenting $G\alpha_q$-dependent endocrine homeostatic and/or neuroprotective $GHSR_{1a}$ functions. Moreover, reductions in $GHSR_{1a}$-mediated βarr signaling (e.g., desensitization, down-regulation) by a G protein–biased agonist should, in principle, minimize tolerance and retain therapeutic efficacy with chronic administration.

To elucidate these hypotheses adequately, future studies will require the development of additional pharmacological tools with distinct signaling properties and, ideally, transgenic animal models that recapitulate both pathway-selective and complete bias in vivo. Fundamentally, if biased signaling can produce desired physiological outcomes with specificity, then biased ligands should provide efficacy with reduced side effects and thereby generate superior drugs. This point has significant theoretical and practical implications for the future of pharmaceutical healthcare, as described recently for the new US Food and Drug Administration (FDA)-approved opioid drug, Olinvyk (74, 75). Importantly, further addressing such issues with the appropriate tools and technologies should reveal whether efficacy-based drug development strategies can be more successful than mechanism-based approaches, as suggested in recent efforts toward drug repurposing across several areas of medicine (76–78).

In summary, we present a functionally selective small molecule $GHSR_{1a}$ ligand that displays unique and favorable pharmacokinetics and pharmacodynamics (PK/PD). With rapidly expanding advances in molecular docking and dynamics, large-scale in silico compound library screening, and the ever-increasing availability of crystal and cryogenic electron microscopy (cryo-EM) structures, GPCR-directed drug discovery/optimization efforts have become more efficient and effective. **N8279** is currently an early lead candidate that can undergo further optimization within this paradigm. Nevertheless, **N8279** and/or its analogs may serve as an important structural scaffold for rationally designing safer and more effective $GHSR_{1a}$-selective treatments to treat DAergic brain diseases, including PD, AD, and/or addictions.

Materials and Methods

Chemicals and Compounds. All chemicals and reagents were purchased from MilliporeSigma or Bio-Techne Corporation, unless indicated otherwise. For details, see *SI Appendix, SI Materials and Methods*.

Animals. All animal studies were performed in accordance with the NIH Guidelines for Animal Care and Use of Laboratory Animals and under protocols approved by the Duke University Animal Care and Use Committee (ACUC) or NIH Division of Veterinary Resources ACUC. Male C57BL/6 mice were used for pharmacokinetic studies and were purchased from Charles River Laboratories. DAT KO mice (51) were backcrossed for >10 generations onto a C57BL/6J (Jackson Laboratory) genetic background. C57BL/6J mice were used also in the novelty and behavioral sensitization experiments. Age- and sex-matched littermate mice between 2 and 6 mo of age were used for all behavioral experiments. Mice were bred and maintained on a standard 12:12 h light:dark cycle, socially housed, and supplied with standard laboratory chow and water ad libitum, except during testing.

NCGC00538279 (N8279) Synthesis. For detailed chemical synthesis procedures of **N8279** (NCATS-SM8864), see *SI Appendix, SI Materials and Methods*.

Cell Culture and Transfections. U2OS, human embryonic kidney (HEK)-293/T, and HEK293/N cells were obtained from the American Type Culture Collection and cultured in Dulbecco's modified Eagle's medium supplemented with 10% (vol/vol) of fetal bovine serum and 1× antibiotic-antimycotic solution (100 IU-1 penicillin, 100 μg/mL streptomycin, and 250 ng/mL amphotericin B; MilliporeSigma). HEK293/S $G\alpha_{q/11}$ KO and its parental WT line were characterized previously (27, 79) and were a generous gift from Dr. Asuka Inoue (Tohoku University). U2OS cells stably expressing 3×HA-$hGHSR_{1a}^{WT}$ and GFP-tagged βarr2 and HEK293/N cells stably expressing 3×HA-$hGHSR_{1a}^{WT}$ and the luminescent Ca^{2+} sensor mitochondrial-Aequorin (miAeq) were made by the Caron laboratory and have been described (20, 21). All cell lines were grown in a humidified incubator at 37 °C (5% CO_2). All transient transfections were performed using a standard calcium phosphate method.

Plasmids. All plasmid constructs were purchased commercially or received as a generous gift from collaborative investigators. For details on plasmid acquisition and cloning procedures, see *SI Appendix, SI Materials and Methods*. Mutagenesis was performed with the QuikChange site-directed mutagenesis kit (Agilent Technologies, Santa Clara, CA).

High-Throughput and Directed Library Compound Screening.
Quantitative high-throughput screening. Quantitative high-throughput screening (qHTS) was performed against ~47,000 compounds from the Sytravon library and the NPC using the PathHunter U2OS $GHSR_{1a}$-βarr1 cells and the βarr Assay Kit (DiscoverX). Prior to the screening, the assay was miniaturized to a 1,536-well format and optimized in terms of signal-to-background window (S/B), Z factor, and potency of ghrelin control. The initial assay validation was performed with Library of Pharmacologically Active Compounds (Sigma-Aldrich) to confirm plate-to-plate reproducibility of parameters, hit rate identification, etc. For qHTS, two doses of the compounds—11 and 57 μM—were used to measure $GHSR_{1a}$ activation using a fully automated robotic screening system (Kalypsys). Briefly, 1.2×10^3 cells were seeded with MultiDrop Combi dispenser (Thermo Fisher Scientific) into white solid-bottom tissue culture–treated 1,536-well plates (Aurora Microplates) in 3 μL of AssayComplete Cell Plating 5 Reagent (DiscoverX) and cultured overnight. Next, 1 μL per well of 1 μM ghrelin diluted in Hanks' balanced salt solution (HBSS) + 10 mM Hepes (HH buffer) was added to one column of the plate, while all other wells were dispensed with 1 μL per well of HH buffer for matching the assay conditions. Subsequently, the libraries' compounds in DMSO solution were transferred from the source plates to the assay plates at 23 nL per well. The plates were incubated for 90 min, followed by addition of 1.5 μL per well PathHunter Detection Reagent prepared according to the manufacturer's instructions. After 60 min of incubation at ambient temperature, the luminescent signal was measured on a ViewLux uHTS Microplate Imager (Perkin-Elmer) with 20 s exposure. Quality of the screening was evaluated based on the median characteristics of Z factor and S/B, which were 0.53 and ~4.5-fold, respectively. Hit detection window parameters were calculated based on results obtained from the vehicle control (EC_0) and ghrelin as the positive control (EC_{100} = 250 nM final concentration) conditions. A cutoff of >60% activation by either the lower or higher compound's dose was used to select primary hits. A follow-up PathHunter U2OS $GHSR_{1a}$ βarr1 assay was performed on 145 selected primary compounds. They were retested at seven doses in the range [57 μM to 3.7 nM], applying the same protocol as for qHTS. Thirty-six hits were selected based on curve response class 1, 2, or 3 for further validation.

X-Ray Diffraction. Single crystal X-ray diffraction studies were conducted on a Bruker Kappa Photon II CPAD diffractometer equipped with Cu K_α radiation (λ = 1.54178 Å). Crystals of the subject compound were grown by dissolving ~1 mg of sample in 350 μL of 90:10 dichloroethane/methanol solution, which was then vapor diffused with Pentane over several days. A 0.267 × 0.243 × 0.228 mm piece of a colorless block was mounted on a Cryoloop with Paratone oil. Data were collected in a nitrogen gas stream at 285 K using ϕ and ϖ scans.

The crystal-to-detector distance was 40 mm using variable exposure time (20 to 90s) depending on θ with a scan width of 2.0°. Data collection was 99.5% complete to 59.009° in θ (0.90 Å). A total of 58,959 reflections were collected, covering the indices $-17 \leq h \leq 17$, $-16 \leq k \leq 16$, and $-24 \leq l \leq 24$. A total of 6,947 reflections were found to be symmetry independent, with an R_{int} of 0.0596. Indexing and unit cell refinement indicated a primitive, monoclinic lattice. The space group was found to be $P2_1/c$. The data were integrated using the Bruker SAINT software program and scaled using the SADABS software program. Solution by direct methods (SHELXT) produced a complete phasing model for refinement. All nonhydrogen atoms were refined anisotropically by full-matrix least-squares (SHELXL-2014). All carbon bonded hydrogen atoms were placed using a riding model. Their positions were constrained relative to their parent atom using the appropriate HFIX command in SHELXL-2014. All other hydrogen atoms (H-bonding) were located in the difference map. Their relative positions were restrained using DFIX commands and their thermals freely refined. Crystallographic data are summarized in *SI Appendix*, Table S2.

$GHSR_{1a}$ Radioligand Binding Assays. [^{125}I]ghrelin-$GHSR_{1a}$ binding assays were performed as described (45), with modifications outlined in *SI Appendix, SI Materials and Methods*.

$G\alpha_q$-Dependent Intracellular Ca^{2+} Mobilization. iCa^{2+} assays were performed as described (21), with modifications described in *SI Appendix, SI Materials and Methods*.

$\beta arr2^{GFP}$ Translocation. $\beta arr2^{GFP}$ translocation assays were performed as described (20), with modifications described in *SI Appendix, SI Materials and Methods*.

NanoBiT-Based $G\alpha_q$ Dissociation and βarr2 Recruitment Assays. $G\alpha_q{}^{LgBiT}$ dissociation assays were performed as described (32), with modifications described in *SI Appendix, SI Materials and Methods*. $^{SmBiT}\beta arr2$ recruitment assays were performed using a modified βarr2 recruitment protocol as described previously (27). Detailed procedures for both NanoBiT assays are described in the *SI Appendix, SI Materials and Methods*.

BRET-Based $G\alpha_q$ Dissociation and βarr2 Recruitment Assays. $G\alpha^{RLuc8}$-$G\gamma^{GFP2}$ dissociation assays (TRUPATH) were performed as originally described (33). $GHSR_{1a}{}^{WT\text{-}RLucII}$ and $GHSR_{1a}{}^{L149G\text{-}RLucII}\_{}^{Venus}\beta arr2$ recruitment assays were performed as described previously (21). Detailed procedures for both BRET assays are described in the *SI Appendix, SI Materials and Methods*.

Chemiluminescent Fixed-Cell ELISA. Quantitative, fixed-cell ELISAs were performed as described (80), but with modification for chemiluminescent detection of surface-expressed $GHSR_{1a}$. A detailed procedure can be found in the *SI Appendix, SI Materials and Methods*.

Bystander BRET. $MyrPalm^{Venus}$ and $2\times FYVE^{Venus}$ bBRET assays were performed as described (38, 40), with modifications described in *SI Appendix, SI Materials and Methods*.

SRF-RE Transcriptional Activity. SRF-RE transcriptional activation assays were performed as described (20), with modifications described in *SI Appendix, SI Materials and Methods*.

Molecular Docking. Molecular docking studies were performed using the Glide and Maestro user interface (Release 2019–4, Schrodinger LLC) as described (81, 82). The model structure of ghrelin-bound $GHSR_{1a}$ (30) and the X-ray crystal structure of antagonist-bound $GHSR_{1a}$ (45) were used to represent the active and inactive state of $GHSR_{1a}$, respectively. The Protein Preparation Wizard function was used to assign bond orders, add hydrogen atoms, and remove water molecules that did not participate in interactions. The $GHSR_{1a}$ models were subjected to energy minimization using the OPLS3 algorithm (A Force Field Providing Broad Coverage of Drug-like Small Molecules and Proteins). A receptor grid box of $30 \times 30 \times 30$ Å^3 with a default inner box ($10 \times 10 \times 10$ Å^3) was centered on the ligand binding pocket. The ligand structures were generated and prepared using the LigPrep function with the OPLS3 force field. Flexible ligand docking was performed using the "standard precision" Glide algorithm, and after the postdocking minimization, the pose with the best docking score was evaluated.

Pharmacokinetic Analysis. Male C57BL/6 mice ($n = 3$/time point) were administered **N8279** at 1 mg/kg IV, 5 mg/kg PO, and 5 mg/kg IP. Plasma, brain, and liver samples were collected over 24 h. **N8279** concentrations in plasma, brain, and liver homogenates were determined by LC-MS/MS. The mean concentration from three animals at each time point was used in the pharmacokinetic (PK) analysis. PK parameters were calculated with Phoenix WinNonlin Software (Ver. 8.0, Certara).

Novelty-Induced Locomotor Activity in DAT KO and Inbred C57BL/6J Mice. Open-field locomotor activity in mice was performed as described (66), with modifications described in *SI Appendix, SI Materials and Methods*.

Cocaine Sensitization. Male and female C57BL6/J mice (Jackson Labs) were administered (IP) vehicle or **N8279** (5 mg/kg) subchronically for 8 consecutive days (once per day) (Fig. 4*D*). Subsequently, mice were placed into the open field (Accuscan Instruments) for 30 min; they were removed, injected (IP) with vehicle or **N8279**, returned to the open field for 30 min, then given (IP) vehicle or cocaine (20 mg/kg) and returned to the open field for 120 min (Fig. 4*D*). This procedure was repeated once per day for 5 consecutive days. A drug-free hiatus in the home cage was imposed for 5 d (washout), and then on day 11, the mice were challenged (IP) with vehicle or cocaine (20 mg/kg) to test for behavioral sensitization. Since the injections of vehicle and **N8279** occurred 30 min prior to cocaine administration, this time period was taken as baseline activity. Since this baseline locomotor activity declined across days in the **N8279** group, the results are presented as percent change from baseline activities.

Statistics. All data are presented as the mean ± SEM derived from multiple independent experiments or animals. For binding and signaling assays, ≥2 technical replicates were included in each experiment. These data were plotted and analyzed in GraphPad Prism version 9.0 with a statistical significance threshold defined as $P < 0.05$. Nonlinear regression parameters and best-fit models for all C/R data were determined statistically by an extra sum-of-squares *F*-test. The behavioral data were analyzed by the appropriate ANOVA followed by a post hoc multiple comparisons test.

Data Availability. All study data are included in the article and/or *SI Appendix*.

ACKNOWLEDGMENTS. We thank Wendy Roberts for the maintenance of the DAT KO and C57BL/6J mouse colonies (Duke University). We also thank Yushi Bai and Lauren Rochelle for performing initial $GHSR_{1a}$ radioligand binding and signaling assays with the hit compounds and the commercial compound library, respectively. We thank the Mouse Behavioral and Neuroendocrine Analysis Core Facility staff for running the behavioral sensitization experiments, with Dr. Ramona M. Rodriguiz statistically analyzing these data (Duke University). Some of the equipment and software used in the behavioral experiments were purchased with a grant from the North Carolina Biotechnology Center. This work has been funded by NIH grants from the National Institute on Drug Abuse, F32DA051139 (J.D.G.), U18DA052417 (L.S.B. and M.G.C.), and P30DA029925 (M.G.C., L.S.B., and K.T.); National Institute of Mental Health grant R37MH073853 (M.G.C.), and National Center for Advancing Translational Sciences grant ZIATR000083 (J.J.M.).

1. M. Kojima *et al.*, Ghrelin is a growth-hormone-releasing acylated peptide from stomach. *Nature* **402**, 656–660 (1999).
2. B. K. Mani, J. M. Zigman, Ghrelin as a survival hormone. *Trends Endocrinol. Metab.* **28**, 843–854 (2017).
3. Y. Sun, P. Wang, H. Zheng, R. G. Smith, Ghrelin stimulation of growth hormone release and appetite is mediated through the growth hormone secretagogue receptor. *Proc. Natl. Acad. Sci. U.S.A.* **101**, 4679–4684 (2004).
4. T. D. Müller *et al.*, Ghrelin. *Mol. Metab.* **4**, 437–460 (2015).
5. D. Serrenho, S. D. Santos, A. L. Carvalho, The role of ghrelin in regulating synaptic function and plasticity of feeding-associated circuits. *Front. Cell. Neurosci.* **13**, 205 (2019).
6. A. Abizaid *et al.*, Ghrelin modulates the activity and synaptic input organization of midbrain dopamine neurons while promoting appetite. *J. Clin. Invest.* **116**, 3229–3239 (2006).
7. Y. Suda *et al.*, Down-regulation of ghrelin receptors on dopaminergic neurons in the substantia nigra contributes to Parkinson's disease-like motor dysfunction. *Mol. Brain* **11**, 6 (2018).
8. E. Jerlhag *et al.*, Ghrelin administration into tegmental areas stimulates locomotor activity and increases extracellular concentration of dopamine in the nucleus accumbens. *Addict. Biol.* **12**, 6–16 (2007).
9. A. H. Morgan, D. J. Rees, Z. B. Andrews, J. S. Davies. Ghrelin mediated neuroprotection – A possible therapy for Parkinson's disease? *Neuropharmacology* **136**, 317–326 (2018).
10. T. Kienast, A. Heinz, Dopamine and the diseased brain. *CNS Neurol. Disord. Drug Targets* **5**, 109–131 (2006).
11. P. G. Strange, Antipsychotic drugs: Importance of dopamine receptors for mechanisms of therapeutic actions and side effects. *Pharmacol. Rev.* **53**, 119–133 (2001).
12. H. You *et al.*, Molecular basis of dopamine replacement therapy and its side effects in Parkinson's disease. *Cell Tissue Res.* **373**, 111–135 (2018).
13. J. R. Schank, A. E. Ryabinin, W. J. Giardino, R. Ciccocioppo, M. Heilig, Stress-related neuropeptides and addictive behaviors: Beyond the usual suspects. *Neuron* **76**, 192–208 (2012).
14. D. Lindholm *et al.*, Current disease modifying approaches to treat Parkinson's disease. *Cell. Mol. Life Sci.* **73**, 1365–1379 (2016).

PHARMACOLOGY

15. S. Yanagi, T. Sato, K. Kangawa, M. Nakazato, The homeostatic force of ghrelin. *Cell Metab.* **27**, 786–804 (2018).
16. W. A. Banks, M. Tschöp, S. M. Robinson, M. L. Heiman, Extent and direction of ghrelin transport across the blood-brain barrier is determined by its unique primary structure. *J. Pharmacol. Exp. Ther.* **302**, 822–827 (2002).
17. M. Schaeffer *et al.*, Rapid sensing of circulating ghrelin by hypothalamic appetite-modifying neurons. *Proc. Natl. Acad. Sci. U.S.A.* **110**, 1512–1517 (2013).
18. A. Edwards, A. Abizaid, Clarifying the ghrelin system's ability to regulate feeding behaviours despite enigmatic spatial separation of the GHSR and its endogenous ligand. *Int. J. Mol. Sci.* **18**, E859 (2017).
19. C. M'Kadmi *et al.*, Agonism, antagonism, and inverse agonism bias at the ghrelin receptor signaling. *J. Biol. Chem.* **290**, 27021–27039 (2015).
20. T. Evron *et al.*, G protein and β-arrestin signaling bias at the ghrelin receptor. *J. Biol. Chem.* **289**, 33442–33455 (2014).
21. K. Toth *et al.*, Encoding the β-arrestin trafficking fate of ghrelin receptor GHSR1a: C-tail-independent molecular determinants in GPCRs. *ACS Pharmacol. Transl. Sci.* **2**, 230–246 (2019).
22. K. Toth *et al.*, Ghrelin receptor antagonism of hyperlocomotion in cocaine-sensitized mice requires βarrestin-2. *Synapse* **72**, e22012 (2018).
23. F. Mende *et al.*, Translating biased signaling in the ghrelin receptor system into differential in vivo functions. *Proc. Natl. Acad. Sci. U.S.A.* **115**, E10255–E10264 (2018).
24. Y. Chebani *et al.*, Enhanced responsiveness of Ghsr Q343X rats to ghrelin results in enhanced adiposity without increased appetite. *Sci. Signal.* **9**, ra39 (2016).
25. W. K. Kroeze *et al.*, PRESTO-Tango as an open-source resource for interrogation of the druggable human GPCRome. *Nat. Struct. Mol. Biol.* **22**, 362–369 (2015).
26. B. Holst, E. Brandt, A. Bach, A. Heding, T. W. Schwartz, Nonpeptide and peptide growth hormone secretagogues act both as ghrelin receptor agonist and as positive or negative allosteric modulators of ghrelin signaling. *Mol. Endocrinol.* **19**, 2400–2411 (2005).
27. L. M. Slosky *et al.*, β-Arrestin-biased allosteric modulator of NTSR1 selectively attenuates addictive behaviors. *Cell* **181**, 1364–1379.e14 (2020).
28. A. Christopoulos, Advances in G protein-coupled receptor allostery: From function to structure. *Mol. Pharmacol.* **86**, 463–478 (2014).
29. L. M. Slosky, M. G. Caron, L. S. Barak, Biased allosteric modulators: New frontiers in GPCR drug discovery. *Trends Pharmacol. Sci.* **42**, 283–299 (2021).
30. B. J. Bender *et al.*, Structural model of ghrelin bound to its G protein-coupled receptor. *Structure* **27**, 537–544.e4 (2019).
31. G. Ferré *et al.*, Structure and dynamics of G protein-coupled receptor-bound ghrelin reveal the critical role of the octanoyl chain. *Proc. Natl. Acad. Sci. U.S.A.* **116**, 17525–17530 (2019).
32. A. Inoue *et al.*, Illuminating G-protein-coupling selectivity of GPCRs. *Cell* **177**, 1933–1947.e25 (2019).
33. R. H. J. Olsen *et al.*, TRUPATH, an open-source biosensor platform for interrogating the GPCR transducerome. *Nat. Chem. Biol.* **16**, 841–849 (2020).
34. K. G. Harikumar *et al.*, Glucagon-like peptide-1 receptor dimerization differentially regulates agonist signaling but does not affect small molecule allostery. *Proc. Natl. Acad. Sci. U.S.A.* **109**, 18607–18612 (2012).
35. A. Saunders *et al.*, Molecular diversity and specializations among the cells of the adult mouse brain. *Cell* **174**, 1015–1030.e16 (2018).
36. R. Granata *et al.*, Acylated and unacylated ghrelin promote proliferation and inhibit apoptosis of pancreatic beta-cells and human islets: Involvement of 3′,5′-cyclic adenosine monophosphate/protein kinase A, extracellular signal-regulated kinase 1/2, and phosphatidyl inositol 3-kinase/Akt signaling. *Endocrinology* **148**, 512–529 (2007).
37. J. D. Violin, X. R. Ren, R. J. Lefkowitz, G-protein-coupled receptor kinase specificity for beta-arrestin recruitment to the beta2-adrenergic receptor revealed by fluorescence resonance energy transfer. *J. Biol. Chem.* **281**, 20577–20588 (2006).
38. J. S. Smith *et al.*, C-X-C motif chemokine receptor 3 splice variants differentially activate beta-arrestins to regulate downstream signaling pathways. *Mol. Pharmacol.* **92**, 136–150 (2017).
39. L. Ménard *et al.*, Synergistic regulation of beta2-adrenergic receptor sequestration: Intracellular complement of beta-adrenergic receptor kinase and beta-arrestin determine kinetics of internalization. *Mol. Pharmacol.* **51**, 800–808 (1997).
40. J. C. Snyder *et al.*, Inhibiting clathrin-mediated endocytosis of the leucine-rich G protein-coupled receptor-5 diminishes cell fitness. *J. Biol. Chem.* **292**, 7208–7222 (2017).
41. A. A. J. Rouault *et al.*, The GPCR accessory protein MRAP2 regulates both biased signaling and constitutive activity of the ghrelin receptor GHSR1a. *Sci. Signal.* **13**, eaax4569 (2020).
42. L. S. Barak, S. Peterson, Modeling of bias for the analysis of receptor signaling in biochemical systems. *Biochemistry* **51**, 1114–1125 (2012).
43. J. Pantel *et al.*, Loss of constitutive activity of the growth hormone secretagogue receptor in familial short stature. *J. Clin. Invest.* **116**, 760–768 (2006).
44. J. Mokrosiński, T. M. Frimurer, B. Sivertsen, T. W. Schwartz, B. Holst, Modulation of constitutive activity and signaling bias of the ghrelin receptor by conformational constraint in the second extracellular loop. *J. Biol. Chem.* **287**, 33488–33502 (2012).
45. Y. Shiimura *et al.*, Structure of an antagonist-bound ghrelin receptor reveals possible ghrelin recognition mode. *Nat. Commun.* **11**, 4160 (2020).
46. B. Holst *et al.*, Overlapping binding site for the endogenous agonist, small-molecule agonists, and ago-allosteric modulators on the ghrelin receptor. *Mol. Pharmacol.* **75**, 44–59 (2009).
47. M. Wheatley *et al.*, Lifting the lid on GPCRs: The role of extracellular loops. *Br. J. Pharmacol.* **165**, 1688–1703 (2012).
48. C. de Graaf, N. Foata, O. Engkvist, D. Rognan, Molecular modeling of the second extracellular loop of G-protein coupled receptors and its implication on structure-based virtual screening. *Proteins* **71**, 599–620 (2008).
49. C. H. Lee, D. Park, D. Wu, S. G. Rhee, M. I. Simon, Members of the Gq alpha subunit gene family activate phospholipase C beta isozymes. *J. Biol. Chem.* **267**, 16044–16047 (1992).
50. E. M. Pfeil *et al.*, Heterotrimeric G protein subunit Gαq is a master switch for Gβγ-mediated calcium mobilization by Gi-coupled GPCRs. *Mol. Cell* **80**, 940–954.e6 (2020).
51. B. Giros, M. Jaber, S. R. Jones, R. M. Wightman, M. G. Caron, Hyperlocomotion and indifference to cocaine and amphetamine in mice lacking the dopamine transporter. *Nature* **379**, 606–612 (1996).
52. S. Mary *et al.*, Heterodimerization with Its splice variant blocks the ghrelin receptor 1a in a non-signaling conformation: A study with a purified heterodimer assembled into lipid discs. *J. Biol. Chem.* **288**, 24656–24665 (2013).
53. A. De Lean, J. M. Stadel, R. J. Lefkowitz, A ternary complex model explains the agonist-specific binding properties of the adenylate cyclase-coupled beta-adrenergic receptor. *J. Biol. Chem.* **255**, 7108–7117 (1980).
54. V. V. Gurevich, R. Pals-Rylaarsdam, J. L. Benovic, M. M. Hosey, J. J. Onorato, Agonist-receptor-arrestin, an alternative ternary complex with high agonist affinity. *J. Biol. Chem.* **272**, 28849–28852 (1997).
55. J. D. McCorvy *et al.*, Structure-inspired design of β-arrestin-biased ligands for aminergic GPCRs. *Nat. Chem. Biol.* **14**, 126–134 (2018).
56. M. Sanchez-Soto *et al.*, A structural basis for how ligand binding site changes can allosterically regulate GPCR signaling and engender functional selectivity. *Sci. Signal.* **13**, eaaw5885 (2020).
57. A. Bock, M. Bermudez, Allosteric coupling and biased agonism in G protein-coupled receptors. *FEBS J.* **288**, 2513–2528 (2021).
58. D. Wacker *et al.*, Structural features for functional selectivity at serotonin receptors. *Science* **340**, 615–619 (2013).
59. D. Wacker *et al.*, Crystal structure of an LSD-bound human serotonin receptor. *Cell* **168**, 377–389.e12 (2017).
60. C. Valant *et al.*, A novel mechanism of G protein-coupled receptor functional selectivity. Muscarinic partial agonist McN-A-343 as a bitopic orthosteric/allosteric ligand. *J. Biol. Chem.* **283**, 29312–29321 (2008).
61. A. Bock *et al.*, The allosteric vestibule of a seven transmembrane helical receptor controls G-protein coupling. *Nat. Commun.* **3**, 1044 (2012).
62. T. Warne, P. C. Edwards, A. G. Leslie, C. G. Tate, Crystal structures of a stabilized β1-adrenoceptor bound to the biased agonists bucindolol and carvedilol. *Structure* **20**, 841–849 (2012).
63. D. Wootten *et al.*, The extracellular surface of the GLP-1 receptor is a molecular trigger for biased agonism. *Cell* **165**, 1632–1643 (2016).
64. T. Kenakin, A. Christopoulos, Signalling bias in new drug discovery: Detection, quantification and therapeutic impact. *Nat. Rev. Drug Discov.* **12**, 205–216 (2013).
65. N. M. Urs *et al.*, Distinct cortical and striatal actions of a β-arrestin-biased dopamine D2 receptor ligand reveal unique antipsychotic-like properties. *Proc. Natl. Acad. Sci. U.S.A.* **113**, E8178–E8186 (2016).
66. L. S. Barak *et al.*, ML314: A biased neurotensin receptor ligand for methamphetamine abuse. *ACS Chem. Biol.* **11**, 1880–1890 (2016).
67. P. J. Wellman, P. S. Clifford, J. A. Rodriguez, Ghrelin and ghrelin receptor modulation of psychostimulant action. *Front. Neurosci.* **7**, 171 (2013).
68. Y. M. Yang, D. S. Kuen, Y. Chung, H. Kurose, S. G. Kim, $G\alpha_{12/13}$ signaling in metabolic diseases. *Exp. Mol. Med.* **52**, 896–910 (2020).
69. N. Suzuki, N. Hajicek, T. Kozasa, Regulation and physiological functions of G12/13-mediated signaling pathways. *Neurosignals* **17**, 55–70 (2009).
70. T. E. Robinson, B. Kolb, Structural plasticity associated with exposure to drugs of abuse. *Neuropharmacology* **47** (Suppl. 1), 33–46 (2004).
71. S. Toda, H. W. Shen, J. Peters, S. Cagle, P. W. Kalivas, Cocaine increases actin cycling: Effects in the reinstatement model of drug seeking. *J. Neurosci.* **26**, 1579–1587 (2006).
72. N. Wettschureck *et al.*, Loss of Gq/11 family G proteins in the nervous system causes pituitary somatotroph hypoplasia and dwarfism in mice. *Mol. Cell. Biol.* **25**, 1942–1948 (2005).
73. T. C. Yin, C. J. Bauchle, A. A. J. Rouault, S. B. Stephens, J. A. Sebag, The insulinostatic effect of ghrelin requires MRAP2 expression in δ cells. *iScience* **23**, 101216 (2020).
74. D. Lambert, G. Calo, Approval of oliceridine (TRV130) for intravenous use in moderate to severe pain in adults. *Br. J. Anaesth.* **125**, e473–e474 (2020).
75. H. S. Tan, A. S. Habib, Oliceridine: A novel drug for the management of moderate to severe acute pain – A review of current evidence. *J. Pain Res.* **14**, 969–979 (2021).
76. S. Pushpakom *et al.*, Drug repurposing: Progress, challenges and recommendations. *Nat. Rev. Drug Discov.* **18**, 41–58 (2019).
77. H. I. Roessler, N. V. A. M. Knoers, M. M. van Haelst, G. van Haaften, Drug repurposing for rare diseases. *Trends Pharmacol. Sci.* **42**, 255–267 (2021).
78. Y. L. Ng, C. K. Salim, J. J. H. Chu, Drug repurposing for COVID-19: Approaches, challenges and promising candidates. *Pharmacol. Ther.* **228**, 107930 (2021).
79. E. Alvarez-Curto *et al.*, Targeted elimination of G proteins and arrestins defines their specific contributions to both intensity and duration of G protein-coupled receptor signaling. *J. Biol. Chem.* **291**, 27147–27159 (2016).
80. S. Pandey, D. Roy, A. K. Shukla, Measuring surface expression and endocytosis of GPCRs using whole-cell ELISA. *Methods Cell Biol.* **149**, 131–140 (2019).
81. Y. Zhou *et al.*, Design of MC1R selective γ-MSH analogues with canonical amino acids leads to potency and pigmentation. *J. Med. Chem.* **60**, 9320–9329 (2017).
82. S. Mowlazadeh Haghighi *et al.*, Replacement of Arg with Nle and modified D-Phe in the core sequence of MSHs, Ac-His-D-Phe-Arg-Trp-NH_2, leads to hMC1R selectivity and pigmentation. *Eur. J. Med. Chem.* **151**, 815–823 (2018).